Broadly neutralizing antibodies targeting a conserved silent face of spike RBD resist extreme SARS-CoV-2 antigenic drift

Authors

Ge Song[1,2,3†], Meng Yuan[4†], Hejun Liu[4†], Tazio Capozzola[1,2,3†], Ryan N. Lin[4], Jonathan L. Torres[4], Wan-ting He[1,2,3], Rami Musharrafieh[1,2,3], Katharina Dueker[1,2,3], Panpan Zhou[1,2,3], Sean Callaghan[1,2,3], Nitesh Mishra[1,2,3], Peter Yong[1,2,3], Fabio Anzanello[1,2,3], Gabriel Avillion[1,2,3], Anh Lina Vo[1,2,3], Xuduo Li[1,2,3], Muzamil Makhdoomi[1], Ziqi Feng[4], Xueyong Zhu[4], Linghang Peng[1], David Nemazee[1], Yana Safonova[5], Bryan Briney[1,2,3], Andrew B Ward[1,2,3,4], Dennis R. Burton[1,2,3,6*], Ian A. Wilson[2,3,4,7*], Raiees Andrabi[1,2,3,8*]

Affiliations

[1]Department of Immunology and Microbiology, The Scripps Research Institute, La Jolla, CA 92037, USA.
[2]IAVI Neutralizing Antibody Center, The Scripps Research Institute, La Jolla, CA 92037, USA
[3]Consortium for HIV/AIDS Vaccine Development (CHAVD), The Scripps Research Institute, La Jolla, CA 92037, USA.
[4]Department of Integrative Structural and Computational Biology, The Scripps Research Institute, La Jolla, CA 92037, USA.
[5]Department of Computer Science, Johns Hopkins University, Baltimore, MD 21218, USA
[6]Ragon Institute of Massachusetts General Hospital, Massachusetts Institute of Technology, and Harvard University, Cambridge, MA 02139, USA.
[7]Skaggs Institute for Chemical Biology, The Scripps Research Institute, La Jolla, CA 92037, USA
[†]These authors contributed equally to this work.
[8]Lead Contact
[*]Corresponding author. Email: burton@scripps.edu (D.R.B.); wilson@scripps.edu (I.A.W.); andrabi@scripps.edu (R.A.).

Summary

Developing broad coronavirus vaccines requires identifying and understanding the molecular basis of broadly neutralizing antibody (bnAb) spike sites. In our previous work, we identified sarbecovirus spike RBD group 1 and 2 bnAbs. We have now shown that many of these bnAbs can still neutralize highly mutated SARS-CoV-2 variants, including the XBB.1.5. Structural studies revealed that group 1 bnAbs use recurrent germline-encoded CDRH3 features to interact with a conserved RBD region that overlaps with class 4 bnAb site. Group 2 bnAbs recognize a less well-characterized "site V" on the RBD and destabilize spike trimer. The site V has remained largely unchanged in SARS-CoV-2 variants and is highly conserved across diverse sarbecoviruses, making it a promising target for broad coronavirus vaccine development. Our findings suggest that targeted vaccine strategies may be needed to induce effective B cell responses to escape resistant subdominant spike RBD bnAb sites.

Introduction

Broadly neutralizing antibody (bnAb) epitope-based vaccines are an important strategy for developing effective interventions against coronaviruses. Among the most potent and dominant neutralizing antibodies (nAbs) elicited in SARS-CoV-2 human infection or vaccination are those targeting the SARS-CoV-2 spike receptor binding domain (RBD) [1-10]. Vaccines that induce these spike RBD nAbs have shown high effectiveness in reducing COVID-19 disease severity and hospitalization [11-14]. However, the emergence of SARS-CoV-2 variants of concern (VOCs) has led to the majority of these RBD-targeting antibodies losing their neutralizing activity [15-24]. The bulk of the mutations on the spikes of SARS-CoV-2 VOCs occur in the RBD region, resulting in substantially reduced potency or loss of neutralizing activity of most clinically approved RBD-targeting nAbs [15,21,25]. This scenario highlights the urgent need to identify bnAbs that can target RBD epitopes that are more highly conserved and resistant to mutation. Such bnAbs are crucial for developing antibody-based interventions and variant-proof vaccines and may also be important against emerging coronaviruses with the potential to seed future pandemics in humans.

RBD nAbs have been classified into 4 major classes, class 1-4, and several subclasses [3,10,26]. Class 1 and 2 RBD antibodies are the most potent and frequently elicited nAbs that target overlapping regions of the receptor binding site (RBS), where the host cell receptor ACE2 binds [3,6,10,26,27]. These nAbs exhibit limited cross-reactivity with related coronaviruses and are easily escaped by SARS-CoV-2 variants [26,27]. Class 3 and 4 RBD

nAbs are less potent and are less frequently elicited in humans but target relatively more conserved regions of the RBD and exhibit cross-reactivity with VOCs and diverse sarbecoviruses [3,26,28-38]. Elicitation of nAb responses that target class 3 and 4 RBD sites or the nearby overlapping nAb epitopes are thus more desirable for broad sarbecovirus vaccine strategies.

In a previous study, we described two sets of RBD bnAbs, group 1 and group 2, that neutralize diverse ACE2-utilizing sarbecoviruses and exhibit binding to clade 2 and 3 non-ACE2 sarbecovirus spike RBDs by targeting more conserved RBD epitopes [34]. Group 1 RBD bnAbs are more potent in neutralization, while group 2 RBD bnAbs show relatively broader binding with different sarbecovirus clades, especially clade 2. Both group 1 and group 2 RBD bnAbs appear to be less frequently elicited in SARS-CoV-2 infection or vaccination and were isolated from two individuals with hybrid immunity (COVID-19 recovered and then vaccinated humans) [34].

In the current study, we investigated the molecular basis of sarbecovirus neutralization breadth by these group 1 and 2 RBD bnAbs and implications for broad vaccine strategies. We first tested the neutralization capacity of a select subset of the most potent and broadest group 1 and group 2 RBD bnAbs with recently emerged SARS-CoV-2 variants. We observed that some of these RBD bnAbs still retain neutralizing activities against highly evolved SARS-CoV-2 variants, including BA.4/5 and XBB.1.5. Group 2 RBD bnAbs were less affected by the more recent Omicron escape mutations. Furthermore, we determined crystal structures of multiple group 1 and group 2 RBD bnAbs to provide a

molecular basis for the broad neutralization of sarbecoviruses and resistance to Omicron neutralization escape. The group 1 RBD bnAbs target a relatively conserved epitope proximal to the class 4 nAb target site or CR3022 cryptic site. The group 2 RBD bnAbs recognize a conserved and relatively 'silent' face of the spike RBD, previously termed site V or lateral site [10]. The group 2 RBD bnAb site V is cryptic on the native-like spike, and bnAbs targeting this site disrupt the spike as a possible mechanism of neutralization. Our data further suggest that both group 1 and 2 RBD bnAb memory B cells may be boostable with bivalent or heterologous SARS spike vaccines towards greater neutralization breadth. Overall, we provide a detailed molecular characterization of RBD bnAb epitopes that could serve as templates for the development of broad coronavirus vaccines, provided that appropriate immunogens can be engineered.

Results

Sarbecovirus spike RBD bnAbs that resist SARS-CoV-2 antigenic escape

As SARS-CoV-2 antibody escape variants continue to emerge, it has become increasingly important to identify bnAbs targeting conserved epitopes that can tolerate the large number of antigenic escape mutations found especially on the Omicron variants. We previously isolated a broad panel of sarbecovirus bnAbs from COVID-19-recovered donors who were subsequently vaccinated [34]. These bnAbs target two distinct regions on the RBD, categorized as group 1 and group 2, based on competition binning studies using SARS-CoV-2 nAbs of known specificities. Group 1 bnAbs compete with RBD class 4 site nAbs and group 2 target a less well-characterized conserved RBD region. Here, to investigate the ability of these bnAbs to resist SARS-CoV-2 escape mutations, we tested the neutralization ability of the group 1 (n = 14) and group 2 (n = 5) RBD bnAbs against a broad panel of SARS-CoV-2 variants including Omicron lineage variants (Figure 1 and Table S1). Group 1 RBD bnAbs were found to be relatively more potent and neutralized the early SARS-CoV-2 variants (Alpha, Beta, Gamma, and Delta) equally efficiently; however, their neutralizing activities dropped substantially against the Omicron variants (Geometric mean IC_{50} change: range = 14 – 105-fold IC_{50} drop) (Figure 1B and Table S1). The most pronounced neutralization loss was observed against BA.2 (geometric mean IC_{50} drop = 105-fold) and BA.2.75 (geometric mean IC_{50} drop = 104-fold) Omicron variants, respectively. Notably, four of the group 1 RBD bnAbs (CC25.3, CC25.36,

CC25.54 and CC84.24) retained neutralizing activity (albeit less potently with Omicron variants) with most or all of the SARS-CoV-2 variants tested (Table S1).

Group 2 RBD bnAbs were shown to have an intrinsically lower neutralization IC_{50} potency, but were comparatively less sensitive to Omicron variant mutations (Geometric mean IC_{50} change: range = 2 – 17-fold IC_{50} drop) (Figure 1C and Table S1). Similar to group 1 RBD bnAbs, neutralization by the group 2 RBD bnAbs was minimally affected against the non-Omicron SARS-CoV-2 variants. One out of five group 2 RBD bnAbs substantially lost neutralization with the Omicron variants (Table S1), but 4 of the 5 group 2 RBD bnAbs (CC25.4, CC25.17, CC25.43 and CC25.56) retained neutralization activities, albeit with IC_{50}'s in the μg/ml range, against most or all of the variants tested. The IC_{50} neutralization changes for these 4 group 2 RBD bnAbs against the SARS-CoV-2 Omicron variants were modest suggesting targeting of spike epitopes that are relatively more resistant to antibody immune escape. The BQ.1.1 variant displayed the most neutralization resistance to group 2 RBD bnAbs compared to the WT SARS-CoV-2 (12-fold drop in geometric mean IC_{50}). Nevertheless, the neutralization activities of 4 group 2 RBD bnAbs remained largely unchanged against the XBB.1.5 variant (Table S1), which is the most dominant SARS-CoV-2 variant (85% infections) circulating in the United States as of April 2023. As a comparison, we also tested 5 RBD nAbs that have been shown to target conserved RBD epitopes [30,32,36,39,40]. Except for class 3 RBD site bnAb, S309, which retained neutralization against the Omicron variants, all other nAbs lost neutralization with these highly resistant SARS-CoV-2 variants (Table S1).

Altogether, we noted that both group 1 and 2 RBD bnAbs, and particularly the group 2 RBD bnAbs can effectively resist the extreme Omicron lineage antigenic drift and represent examples of human bnAbs that still retain substantial neutralizing activity with these highly evolved SARS-CoV-2 variants. These features support the potential utilization of group 1 and 2 RBD bnAbs in antibody-based interventions and as templates for variant-proof SARS-CoV-2 vaccines.

Somatic hypermutation in RBD bnAbs is critical for neutralization of Omicron lineage variants

To investigate the role of antibody somatic hypermutation (SHM) in virus neutralization by group 1 and 2 RBD bnAbs, we generated inferred germline (iGL) versions by reverting their heavy and light chains to the corresponding germlines. The iGL heavy and light chain V, D and J regions were reverted back to their germline genes, while the non-templated N-additions at V/(D)/J junctions remained the same as in the mature bnAb versions, as described previously [41] (Figure 2A). It is not possible to revert the non-templated CDR3 junctional regions in the iGLs and these regions may potentially contribute to neutralization. Therefore, the iGLs primarily allow us to assess the contribution of the SHMs in the templated V-D-J regions for neutralization. We evaluated the mature group 1 and 2 RBD bnAbs and their iGL versions against SARS-CoV-2 variants. We noted that while many of the group 1 RBD bnAb iGLs retain neutralization with less mutated SARS-CoV-2 variants (Alpha, Beta, Gamma and Delta), they fail to neutralize the more evolved Omicron variants (Figure 2B and Table S1). In comparison the group 2 RBD bnAb iGLs

fail to neutralize any of the SARS-CoV-2 variants (Figure 2C and Table S1). We also tested these group 1 and group 2 RBD bnAbs and their iGLs with ACE2-utilizing clade 1b (Pang17) and clade 1a (SARS-CoV-1 and WIV1) sarbecoviruses [42,43]. We noted that, while most mature bnAbs neutralized these sarbecoviruses, as reported previously [34], some iGLs of group 1 RBD bnAbs retained neutralization, especially with WIV1 and Pang 17 (Table S1). These results suggest that human antibodies in their germline configurations are able to recognize these sarbecovirus spikes, as also noted by other studies [44].

Overall, the findings suggest that germline residues in group 1 RBD bnAbs may contribute to neutralization of SARS-CoV-2 and its minimally mutated variants. However, SHMs for both group 1 and 2 RBD bnAbs are required to neutralize more evolved SARS-CoV-2 Omicron lineage variants.

Group 1 and 2 RBD bnAb memory B cells and potential recall boosts

To investigate whether group 1 and 2 RBD bnAbs bind to SARS-CoV-2 Omicron BA.4/5 spike and other clades of sarbecovirus spikes for potential boost considerations, we tested their binding to various spikes and their corresponding RBDs by BioLayer Interferometry (BLI). The BA.4/5 Omicron spike is a component of the current SARS-CoV-2 bivalent booster vaccines [45,46]. Therefore, we first assessed whether the group 1 and 2 RBD bnAbs can bind to the BA.4/5 Omicron spike and whether their memory B cells are likely to be boosted by the current bivalent vaccines. As expected from the neutralization

results, both group 1 and 2 RBD bnAbs showed strong binding to the SARS-CoV-2 spike protein (Figure 2D-E and Table S2). Consistent with the neutralization of BA.4/5 Omicron variant above, the binding of group 1 RBD bnAbs was significantly reduced against the BA.4/5 Omicron spike (Figure 2D). Nevertheless, many group 1 RBD bnAbs, especially the ones that neutralize BA.4/5 variant still bound to its spike protein with high affinity (Figure 2D and Table S2). In comparison, the group 2 RBD bnAbs bound to BA.4/5 Omicron spike equally efficiently (Figure 2E and Table S2). The findings suggest that majority of both group 1 and 2 RBD bnAbs are likely to be boosted with the BA.4/5 bivalent vaccine.

We further tested the binding by group 1 and 2 RBD bnAbs to spike proteins derived from heterologous clade 1a (SARS-CoV-1), clade 2 (RmYN02) and clade 3 (BM-4831) sarbecoviruses [34,42,47]. The group 1 RBD bnAb showed substantially reduced binding to SARS-CoV-1 and RmYN02 compared to the SARS-CoV-2 spike but the binding with sarbecovirus clade 3 BM-4831 spike was comparable (Figure 2D and Table S2). Most of the group 2 RBD bnAbs showed strong binding to the clade 2 (RmYN02) and clade 3 (BM-4831) sarbecovirus spike-derived proteins (Figure 2E and Table S2). The results suggest that heterologous clades 2 and 3 spike-derived protein immunogens could be utilized to boost group 1 and 2 RBD bnAb responses, and specifically the clade 3 BM-4831 spike immunogen may recall group 1 RBD bnAb memory B cells more efficiently. We also tested the group 1 and 2 RBD bnAbs with RBD of SARS-CoV-2, BA.4/5 Omicron and the heterologous clade 1a, 2 and 3 sarbecoviruses (SARS-CoV-1, RmYN02 and BM-

4831). The binding responses were overall lower but largely consistent with corresponding spike binding with some exceptions (Figure 2D-E and Table S2).

Overall, we observed that the binding of group 1 RBD bnAbs with BA.4/5 Omicron and heterologous sarbecovirus spikes was substantially reduced as compared to the parental SARS-CoV-2 but binding by group 2 RBD bnAbs were comparable. Nevertheless, both groups of bnAbs are likely boostable by these spikes.

To gain more insight into the detailed binding modes of group 1 and 2 bnAbs, we selected four antibodies from group 1 and three antibodies from group 2 to perform detailed structural studies as described below.

Structures of group 1 bnAbs complexed to SARS-CoV-2 RBD show a recurrent YYDRxG feature in CDRH3 and diverse light chain interactions

Six of the 14 antibodies from group 1 RBD bnAbs shared the same YYDRxG motif encoded by IGHD3-22 that we and others previously identified [34,48,49]. These YYDRxG antibodies exhibited broad neutralization breadth against SARS-CoV-2 variants, including Omicron subvariants (Table S1). Two additional antibodies featuring a YYDSSG motif, a germline precursor of the YYDRxG motif [48], showed cross-reactive binding to, but no neutralization of, Omicron variants.

To understand the basis for the superior breadth of YYDRxG antibodies, we determined crystal structures of three antibodies, CC25.54, CC84.24, and CC84.2, in complex with SARS-CoV-2 RBD with resolutions ranging from 2.9 to 3.1 Å (Figure 3A-C and Table S3). The structures revealed that the antibodies bind the CR3022 cryptic site using similar approach angles that allow them to compete with ACE2 binding even through there is no or minor epitope overlap (Figure 3D-E and Figure S1). The approach angle is also similar to that identified previously for YYDRxG antibodies [10,48,49]. Analysis of the buried surface area (BSA) on SARS-CoV-2 RBD by these antibodies using the PISA program found similar overall BSA, although the percentage of light chain BSA varies among different antibodies (Figure 3F and Figure S1). Further inspection of the antibody-antigen interactions showed variable contacts of the antibody light chains with SARS-CoV-2 RBD, while the heavy chain CDR3 maintained essentially the same contacts. The light chain of CC84.2 contributes a larger BSA compared to CC25.54 and CC84.24, involving CDRs L1 and L2 of the antibody (Figure 3F and Figure S2). Different germline genes encoding the light chains of these YYDRxG antibodies are responsible for the different interactions. CC84.2 is encoded by IGKV3-20, while CC25.54 and CC84.24 are encoded by IGLV3-21 and IGKV1-5, respectively.

A YYDML motif enables group 1 RBD bnAb CC25.36 to bind SARS-CoV-2 RBD in a similar approach angle as YYDRxG antibodies.

Another group 1 antibody, CC25.36, showed comparable breadth as the YYDRxG antibodies. The crystal structure of CC25.36 revealed that the antibody binds SARS-CoV-

2 RBD at the same CR3022 cryptic site on SARS-CoV-2 RBD, which appears less sensitive to mutations in Omicron strains (Figure 4A, Tables S1 and S2). Structural overlay illustrated that CC25.36 uses a similar approach angle to YYDRxG antibodies (Figure 4D). Further inspection showed that a YYDML motif in CC25.36 binds to approximately the same site as the YYDRxG motif in the other antibodies but with different interactions (Figure 4B and Figure S2). The $_{99}$YY$_{100}$ dipeptide in the YYDML motif binds with similar interactions as in the YYDRxG motif, which probably determines the site specificity of antibody binding (Figure 4B); the other RBD interactions with CDRH3 differ from the YYDRxG antibodies. D100a forms internal hydrogen bonds with the backbone of $_{100b}$ML$_{100c}$ as well as SARS-CoV-2 RBD K378. $_{100b}$ML$_{100c}$ interacts with a hydrophobic patch formed by RBD Y369, F374, and F378. PISA analysis confirmed that the light chain of CC25.36 contributes a large BSA similar to CC84.2 (Figure 4C and Figure S2). Structural superimposition on SARS-CoV-2 RBD showed that the CC25.36 light chain is positioned in the same way as CC84.2, although the CC25.36 light chain is encoded by the IGLV1-40 gene. A homology search for the YYDML motif showed that YYDIL or YYDLL motifs, also encoded by IGHD3-9, are present in other SARS-CoV-2 antibodies, e.g., COV2-2258 [8], C531 [50], and C2179 [51]. However, whether they bind to the same epitope as CC25.36 warrants further investigation by structural studies.

Structural studies of group-2 RBD broadly neutralizing antibodies

In our previous study of monoclonal antibodies from COVID-19 recovered-vaccinated donors [34], the group-2 antibodies exhibited little or no competition with receptor binding site (RBS) antibodies. Group-2 antibodies showed impressive neutralization breadth

against sarbecoviruses including SARS-CoV-2, SARS-CoV-1, Pang17, WIV1, and SHC014 [34]. Here we show that group 2 antibodies neutralize all SARS-CoV-2 variants to date, including Wuhan, early variants, and Omicron subvariants BA.1, BA.2, BA.5, BQ.1.1, and XBB.1.5 (Table S1). To understand the molecular basis of these broadly neutralizing antibodies, we determined crystal structures of SARS-CoV-2 RBD in complex with three group 2 antibodies, CC25.4, CC25.56 and CC25.43, at resolutions of 1.79 Å, 2.84 Å, and 2.71 Å, respectively (Figure 5 and Table S3). The crystal structures revealed that all three antibodies target a cryptic region on the RBD immediately below the ridge region (Figure 5A). This site has been referred to as 'site V' [31], 'left flank' [52], or 'E3' [19] in previous studies, and does not overlap with the RBS (Figure 5A) or compete with ACE2 binding (Figures S2A and Figure S3).

All three site V antibodies target the RBD using all six CDRs of their heavy and light chains (Figure 5A, 5B and Figure S4). For CC25.4 CDRs H1 and H2, V_H T30 hydrogen bonds with RBD-R357, and V_H D53 with RBD-N394. CDR H3 interacts extensively with the RBD (Figure 5B). For example, V_H E97 makes a salt bridge with RBD-R466, and V_H M100a and Y100d form hydrophobic and aromatic interactions with RBD-Y396, F429, P426, and F464. For the light chain, V_L N31 and D93 engage RBD-K462 through a hydrogen bond and salt bridge and other HBs are made with V_L N52 and K96 to the RBD (Figure 5B). For CC25.43, the heavy chain dominates the interaction with RBD and is responsible for 82% of BSA. All three HCDR loops interact with RBD. RBD-R357 forms a CH-pi bond with V_H Y100, whose main chain interacts with RBD-R355, which in turn forms a salt bridge with D398. RBD-R357 is also clamped by salt bridges to two acidic residues in the

light chain, V_L D92, and D94. In CC25.56, CDRs H1 and H2 engage in extensive polar interactions with the RBD. V_H R31 forms a salt bridge with RBD-D428, and K462 forms two salt bridges with V_H D54 and D56. The hydrophobic tip of CDR H3 is comprised of V_H I97, A98, and V99, which interact with RBD-W353 and F464. The light chain also forms extensive interactions with the RBD.

RBDs on the SARS-CoV-2 S-protein flip between up and down conformations, where an RBD in the up conformation can engage with the host receptor ACE2, expose more epitope area, and also elicit antibodies specific to up-only conformations. In either up- or down-conformation, the S-protein can retain an intact pre-fusion state. However, our structures showed that the site V antibodies target a cryptic site on the RBD. Antibody binding to this epitope would clash with N-terminal domain (NTD) in the adjacent protomer of the S trimer, even if the RBD is in an up conformation when modeled on a pre-fusion SARS-CoV-2 S structure (Figure 5C). This observation suggests that binding of these site V antibodies may result in a conformational rearrangement of the RBD relative to the NTD in the S trimer in the pre-fusion state that could possibly affect viral entry.

Most SARS-CoV-2 RBD antibodies target three regions: the RBS, the CR3022 site, and the S309 site (Figure 6A). Antibodies targeting the RBS generally exhibit higher frequency and higher neutralization potency due to direct competition with receptor [29]. Almost all commercially available therapeutic neutralizing antibodies (except for Sotrovimab) for COVID-19 treatment target the RBS. However, the RBS is highly variable among sarbecoviruses and SARS-CoV-2 variants (Figures 6A). In fact, all of these therapeutic

antibodies have now been evaded by at least one SARS-CoV-2 variant. Here we show that the epitope region of CC25.4, CC25.43, and CC25.56 is highly conserved among sarbecoviruses (Figures 6A-B). Indeed, epitope residues of CC25.4 and CC25.56 are 100% conserved among all SARS-CoV-2 variants to date, while only one mutation (R346T) in BQ.1.1 and XBB.1.5 is located in the CC25.43 epitope (Figure 6B). The high conservation of site V explains the observation that antibodies that target this region largely retain neutralization activity against SARS-CoV-2 variants and other sarbecoviruses (Figure 1B and Table S1) [34]. In addition, in contrast to some other sites accommodating public antibodies, such as RBS-A targeted by IGHV3-53 and IGHV1-58 antibodies [6,53], RBS-B by IGHV1-2 antibodies [6], RBS-D by IGHV2-5 antibodies [6], and S2 stem by IGHV1-46 antibodies [54,55], IgBLAST analysis [56] showed that antibodies targeting site V are encoded by various germlines and no public antibodies have yet been discovered (Figure 6C).

To further determine the epitopes recognized by group 2 RBD bnAbs in the soluble spike, we employed single-particle negative stain electron microscopy to image the complexes of SARS-CoV-2 spike and bnAb Fabs (Figure 7). NsEM complexes revealed Fab-induced SARS-CoV-2 spike destabilization with CC25.43 resulting into 100% dimer particles while CC25.4 and CC25.56 showed an approximate 50/50 mix of spike dimer vs. trimer (Figure 7A-C). Particles were unable to converge in 3D due to heterogeneity; therefore, we were unable to produce 3D maps of the spike-antibody complexes. Notably, from the CC25.56 complex, we observed initial binding of antibody to the spike trimers, which quickly dissociated into dimers. Consistent with our crystallography structures, the EM studies

revealed that group 2 RBD bnAbs bind to a cryptic face of RBD to destabilize the spike trimer. The findings are suggestive of antibody mediated spike destabilization as putative mechanism of neutralization for group 2 RBD bnAbs.

Discussion

The emergence of antibody escape variants of the SARS-CoV-2 Omicron lineage has led to an urgent search for new bnAbs that target conserved spike epitopes. These bnAbs could be used in antibody-mediated prophylaxis or therapy and serve as templates for broad coronavirus vaccine strategies. In this study, we investigated the molecular basis of bnAbs that target conserved spike RBD sites, providing detailed information on the sites that resist virus escape. Our findings will aid in the design of pan-sarbecovirus vaccines.

Here, we revealed that YYDRxG antibodies from group 1 RBD bnAbs (i.e., CC25.54, CC84.24, and CC84.2) target the CR3022 conserved site using essentially the same approach angles as one another, consistent with our previous analysis [48]. The binding of these antibodies to SARS-CoV-2 RBD sterically clashes with ACE2 binding, although the epitope footprint of these antibodies does not overlap with the ACE2 footprint. The structures demonstrate that diverse light chains permit antibody neutralization. With more interactions between the light chain and SARS-CoV-2 RBD compared to CC25.54 and CC84.24, CC84.2 can neutralize VOCs without somatic hypermutation. We also determined the crystal structure of CC25.36, which binds SARS-CoV-2 with virtually the

same approach angle as YYDRxG antibodies and neutralized the virus using the same mechanism as those antibodies. Like CC84.2, the CC25.36 light chain has more contacts compared to CC25.54 and CC84.24, and its inferred germline version showed broad neutralization against VOCs. A newly observed binding motif, YYDML, encoded by IGHD3-9 in CC25.36 CDRH3, binds the same site as the YYDRxG motif but with distinct interactions, which could potentially be a shared motif targeting the CR3022 site. Homology sequence search revealed other potent SARS-CoV-2 RBD Abs, such as COV2-2258 [8], C531 [50], and C2179 [51], share the YYDIL or YYDLL sequences in CDRH3 encoded by IGHD3-9. Further structural studies are needed to determine how similar the binding modes of these antibodies are to that of CC25.36, particularly comparisons of the interaction of YYDIL and YYDLL motifs and the YYDML motif of CC25.36. Overall, multiple antibody germline solutions of group 1 bnAbs converge to recognize a common conserved RBD bnAb site typified by class 4 epitope targeting mAb, CR3022.

In terms of group 1 RBD bnAb B cell precursors, immunogen design strategies could take advantage of the germline-encoded CDRH3 features for vaccine targeting that are described here [57-61]. One potential challenge is that the immunodominant class 1 and 2 RBS nAbs responses may compete with the group 1 RBD bnAb responses. Accordingly, rational immunogen design may seek to effectively mask the RBS directed strain specific nAb responses, while still favorably exposing the RBD group 1 bnAb site to elicit the desired responses.

We also show that group 2 bnAbs, CC25.4, CC25.43, and CC25.56 target another highly conserved region of the RBD, namely site V, with very few mutations in this site in SARS-CoV-2 variants to date. This epitope region is juxtaposed to the neighboring NTD and likely stabilizes both the up and down conformations of the RBD. Structural and functional roles of this site may therefore be the cause of its extremely low variation. A few previously reported human neutralizing antibodies including S2H97 [31], COVOX-45 [52], 553-49 [62], and XMA09 [63] also target this site (Figure S3C) and exhibit remarkably broad neutralization. RBD resurfacing strategies to mask the immunodominant B cell epitopes and immunofocus B cell responses to the site V may be rewarding to induce group 2 bnAb responses (refs).

In addition to site V, some other highly conserved sites on SARS-CoV-2 S have been discovered to be targeted by neutralizing antibodies, including the S2 stem helix [54,55,64-66] and fusion peptide [67-69]. Although these sites are well conserved, and therefore can bind antibodies with high breadth, the neutralization potency of these antibodies is usually within the medium-to-low range, potentially due to their indirect neutralizing mechanisms or relative inaccessibility that may require conformational breathing or local rearrangements to permit antibody binding. Further affinity maturation may be required to confer higher neutralizing potency to these broad antibodies.

Overall, our study presents a comprehensive molecular characterization of RBD bnAb epitopes, which can potentially serve as blueprints for the design of broad coronavirus vaccines.

422

Reference:

1. Wang, Z., Schmidt, F., Weisblum, Y., Muecksch, F., Barnes, C.O., Finkin, S., Schaefer-Babajew, D., Cipolla, M., Gaebler, C., Lieberman, J.A., et al. (2021). mRNA vaccine-elicited antibodies to SARS-CoV-2 and circulating variants. Nature *592*, 616-622. 10.1038/s41586-021-03324-6.
2. Greaney, A.J., Loes, A.N., Gentles, L.E., Crawford, K.H.D., Starr, T.N., Malone, K.D., Chu, H.Y., and Bloom, J.D. (2021). Antibodies elicited by mRNA-1273 vaccination bind more broadly to the receptor binding domain than do those from SARS-CoV-2 infection. Science translational medicine *13*, eabi9915. 10.1126/scitranslmed.abi9915.
3. Barnes, C.O., Jette, C.A., Abernathy, M.E., Dam, K.A., Esswein, S.R., Gristick, H.B., Malyutin, A.G., Sharaf, N.G., Huey-Tubman, K.E., Lee, Y.E., et al. (2020). SARS-CoV-2 neutralizing antibody structures inform therapeutic strategies. Nature *588*, 682-687. 10.1038/s41586-020-2852-1.
4. Barnes, C.O., West, A.P., Jr., Huey-Tubman, K.E., Hoffmann, M.A.G., Sharaf, N.G., Hoffman, P.R., Koranda, N., Gristick, H.B., Gaebler, C., Muecksch, F., et al. (2020). Structures of Human Antibodies Bound to SARS-CoV-2 Spike Reveal Common Epitopes and Recurrent Features of Antibodies. Cell *182*, 828-842 e816. 10.1016/j.cell.2020.06.025.
5. Rogers, T.F., Zhao, F., Huang, D., Beutler, N., Burns, A., He, W.T., Limbo, O., Smith, C., Song, G., Woehl, J., et al. (2020). Isolation of potent SARS-CoV-2 neutralizing antibodies and protection from disease in a small animal model. Science *369*, 956-963. 10.1126/science.abc7520.
6. Yuan, M., Liu, H., Wu, N.C., Lee, C.D., Zhu, X., Zhao, F., Huang, D., Yu, W., Hua, Y., Tien, H., et al. (2020). Structural basis of a shared antibody response to SARS-CoV-2. Science *369*, 1119-1123. 10.1126/science.abd2321.
7. Robbiani, D.F., Gaebler, C., Muecksch, F., Lorenzi, J.C.C., Wang, Z., Cho, A., Agudelo, M., Barnes, C.O., Gazumyan, A., Finkin, S., et al. (2020). Convergent antibody responses to SARS-CoV-2 in convalescent individuals. Nature *584*, 437-442. 10.1038/s41586-020-2456-9.
8. Zost, S.J., Gilchuk, P., Chen, R.E., Case, J.B., Reidy, J.X., Trivette, A., Nargi, R.S., Sutton, R.E., Suryadevara, N., Chen, E.C., et al. (2020). Rapid isolation and profiling of a diverse panel of human monoclonal antibodies targeting the SARS-CoV-2 spike protein. Nature medicine *26*, 1422-1427. 10.1038/s41591-020-0998-x.
9. Brouwer, P.J.M., Caniels, T.G., van der Straten, K., Snitselaar, J.L., Aldon, Y., Bangaru, S., Torres, J.L., Okba, N.M.A., Claireaux, M., Kerster, G., et al. (2020). Potent neutralizing antibodies from COVID-19 patients define multiple targets of vulnerability. Science *369*, 643-650. 10.1126/science.abc5902.
10. Liu, H., and Wilson, I.A. (2022). Protective neutralizing epitopes in SARS-CoV-2. Immunological reviews *310*, 76-92. 10.1111/imr.13084.
11. Lopez Bernal, J., Gower, C., and Andrews, N. (2021). Effectiveness of Covid-19 Vaccines against the B.1.617.2 (Delta) Variant. Reply. The New England journal of medicine *385*, e92. 10.1056/NEJMc2113090.
12. Abu-Raddad, L.J., Chemaitelly, H., and Butt, A.A. (2021). Effectiveness of the BNT162b2 Covid-19 Vaccine against the B.1.1.7 and B.1.351 Variants. The New England journal of medicine *385*, 187-189. 10.1056/NEJMc2104974.
13. Polack, F.P., Thomas, S.J., Kitchin, N., Absalon, J., Gurtman, A., Lockhart, S., Perez, J.L., Pérez Marc, G., Moreira, E.D., Zerbini, C., et al. (2020). Safety and Efficacy of the BNT162b2 mRNA Covid-19 Vaccine. New England Journal of Medicine *383*, 2603-2615. 10.1056/NEJMoa2034577.

14. Baden, L.R., El Sahly, H.M., Essink, B., Kotloff, K., Frey, S., Novak, R., Diemert, D., Spector, S.A., Rouphael, N., Creech, C.B., et al. (2020). Efficacy and Safety of the mRNA-1273 SARS-CoV-2 Vaccine. New England Journal of Medicine *384*, 403-416. 10.1056/NEJMoa2035389.
15. Wang, Q., Iketani, S., Li, Z., Liu, L., Guo, Y., Huang, Y., Bowen, A.D., Liu, M., Wang, M., Yu, J., et al. (2023). Alarming antibody evasion properties of rising SARS-CoV-2 BQ and XBB subvariants. Cell *186*, 279-286.e278. 10.1016/j.cell.2022.12.018.
16. Wang, Q., Guo, Y., Iketani, S., Nair, M.S., Li, Z., Mohri, H., Wang, M., Yu, J., Bowen, A.D., Chang, J.Y., et al. (2022). Antibody evasion by SARS-CoV-2 Omicron subvariants BA.2.12.1, BA.4 and BA.5. Nature *608*, 603-608. 10.1038/s41586-022-05053-w.
17. Liu, L., Iketani, S., Guo, Y., Chan, J.F., Wang, M., Liu, L., Luo, Y., Chu, H., Huang, Y., Nair, M.S., et al. (2022). Striking antibody evasion manifested by the Omicron variant of SARS-CoV-2. Nature *602*, 676-681. 10.1038/s41586-021-04388-0.
18. Iketani, S., Liu, L., Guo, Y., Liu, L., Chan, J.F., Huang, Y., Wang, M., Luo, Y., Yu, J., Chu, H., et al. (2022). Antibody evasion properties of SARS-CoV-2 Omicron sublineages. Nature *604*, 553-556. 10.1038/s41586-022-04594-4.
19. Cao, Y., Yisimayi, A., Jian, F., Song, W., Xiao, T., Wang, L., Du, S., Wang, J., Li, Q., Chen, X., et al. (2022). BA.2.12.1, BA.4 and BA.5 escape antibodies elicited by Omicron infection. Nature *608*, 593-602. 10.1038/s41586-022-04980-y.
20. Cao, Y., Song, W., Wang, L., Liu, P., Yue, C., Jian, F., Yu, Y., Yisimayi, A., Wang, P., Wang, Y., et al. (2022). Characterization of the enhanced infectivity and antibody evasion of Omicron BA.2.75. Cell host & microbe *30*, 1527-1539.e1525. 10.1016/j.chom.2022.09.018.
21. Cao, Y., Jian, F., Wang, J., Yu, Y., Song, W., Yisimayi, A., Wang, J., An, R., Chen, X., Zhang, N., et al. (2023). Imprinted SARS-CoV-2 humoral immunity induces convergent Omicron RBD evolution. Nature *614*, 521-529. 10.1038/s41586-022-05644-7.
22. Hachmann, N.P., Miller, J., Collier, A.Y., and Barouch, D.H. (2022). Neutralization Escape by SARS-CoV-2 Omicron Subvariant BA.4.6. The New England journal of medicine *387*, 1904-1906. 10.1056/NEJMc2212117.
23. Planas, D., Saunders, N., Maes, P., Guivel-Benhassine, F., Planchais, C., Buchrieser, J., Bolland, W.H., Porrot, F., Staropoli, I., Lemoine, F., et al. (2022). Considerable escape of SARS-CoV-2 Omicron to antibody neutralization. Nature *602*, 671-675. 10.1038/s41586-021-04389-z.
24. Wang, Q., Li, Z., Ho, J., Guo, Y., Yeh, A.Y., Mohri, H., Liu, M., Wang, M., Yu, J., Shah, J.G., et al. (2022). Resistance of SARS-CoV-2 omicron subvariant BA.4.6 to antibody neutralisation. Lancet Infect Dis *22*, 1666-1668. 10.1016/s1473-3099(22)00694-6.
25. Westendorf, K., Žentelis, S., Wang, L., Foster, D., Vaillancourt, P., Wiggin, M., Lovett, E., van der Lee, R., Hendle, J., Pustilnik, A., et al. (2022). LY-CoV1404 (bebtelovimab) potently neutralizes SARS-CoV-2 variants. Cell reports *39*, 110812. 10.1016/j.celrep.2022.110812.
26. Yuan, M., Huang, D., Lee, C.D., Wu, N.C., Jackson, A.M., Zhu, X., Liu, H., Peng, L., van Gils, M.J., Sanders, R.W., et al. (2021). Structural and functional ramifications of antigenic drift in recent SARS-CoV-2 variants. Science *373*, 818-823. 10.1126/science.abh1139.
27. Wang, Z., Muecksch, F., Schaefer-Babajew, D., Finkin, S., Viant, C., Gaebler, C., Hoffmann, H.H., Barnes, C.O., Cipolla, M., Ramos, V., et al. (2021). Naturally enhanced neutralizing breadth against SARS-CoV-2 one year after infection. Nature *595*, 426-431. 10.1038/s41586-021-03696-9.
28. Yuan, M., Wu, N.C., Zhu, X., Lee, C.D., So, R.T.Y., Lv, H., Mok, C.K.P., and Wilson, I.A. (2020). A highly conserved cryptic epitope in the receptor binding domains of SARS-CoV-2 and SARS-CoV. Science *368*, 630-633. 10.1126/science.abb7269.

29. Yuan, M., Zhu, X., He, W.T., Zhou, P., Kaku, C.I., Capozzola, T., Zhu, C.Y., Yu, X., Liu, H., Yu, W., et al. (2022). A broad and potent neutralization epitope in SARS-related coronaviruses. Proceedings of the National Academy of Sciences of the United States of America *119*, e2205784119. 10.1073/pnas.2205784119.
30. Li, D., Edwards, R.J., Manne, K., Martinez, D.R., Schafer, A., Alam, S.M., Wiehe, K., Lu, X., Parks, R., Sutherland, L.L., et al. (2021). In vitro and in vivo functions of SARS-CoV-2 infection-enhancing and neutralizing antibodies. Cell *184*, 4203-4219 e4232. 10.1016/j.cell.2021.06.021.
31. Starr, T.N., Czudnochowski, N., Liu, Z., Zatta, F., Park, Y.J., Addetia, A., Pinto, D., Beltramello, M., Hernandez, P., Greaney, A.J., et al. (2021). SARS-CoV-2 RBD antibodies that maximize breadth and resistance to escape. Nature *597*, 97-102. 10.1038/s41586-021-03807-6.
32. Pinto, D., Park, Y.J., Beltramello, M., Walls, A.C., Tortorici, M.A., Bianchi, S., Jaconi, S., Culap, K., Zatta, F., De Marco, A., et al. (2020). Cross-neutralization of SARS-CoV-2 by a human monoclonal SARS-CoV antibody. Nature *583*, 290-295. 10.1038/s41586-020-2349-y.
33. Rappazzo, C.G., Tse, L.V., Kaku, C.I., Wrapp, D., Sakharkar, M., Huang, D., Deveau, L.M., Yockachonis, T.J., Herbert, A.S., Battles, M.B., et al. (2021). Broad and potent activity against SARS-like viruses by an engineered human monoclonal antibody. Science *371*, 823-829. 10.1126/science.abf4830.
34. He, W.-t., Musharrafieh, R., Song, G., Dueker, K., Tse, L.V., Martinez, D.R., Schäfer, A., Callaghan, S., Yong, P., Beutler, N., et al. (2022). Targeted isolation of diverse human protective broadly neutralizing antibodies against SARS-like viruses. Nature immunology *23*, 960-970. 10.1038/s41590-022-01222-1.
35. He, W.-t., Yuan, M., Callaghan, S., Musharrafieh, R., Song, G., Silva, M., Beutler, N., Lee, W.-H., Yong, P., Torres, J.L., et al. (2022). Broadly neutralizing antibodies to SARS-related viruses can be readily induced in rhesus macaques. Science translational medicine *14*, eabl9605. doi:10.1126/scitranslmed.abl9605.
36. Jette, C.A., Cohen, A.A., Gnanapragasam, P.N.P., Muecksch, F., Lee, Y.E., Huey-Tubman, K.E., Schmidt, F., Hatziioannou, T., Bieniasz, P.D., Nussenzweig, M.C., et al. (2021). Broad cross-reactivity across sarbecoviruses exhibited by a subset of COVID-19 donor-derived neutralizing antibodies. Cell reports *36*, 109760. 10.1016/j.celrep.2021.109760.
37. Martinez, D.R., Schafer, A., Gobeil, S., Li, D., De la Cruz, G., Parks, R., Lu, X., Barr, M., Stalls, V., Janowska, K., et al. (2021). A broadly cross-reactive antibody neutralizes and protects against sarbecovirus challenge in mice. Science translational medicine, eabj7125. 10.1126/scitranslmed.abj7125.
38. Deshpande, A., Harris, B.D., Martinez-Sobrido, L., Kobie, J.J., and Walter, M.R. (2021). Epitope Classification and RBD Binding Properties of Neutralizing Antibodies Against SARS-CoV-2 Variants of Concern. Frontiers in immunology *12*, 691715. 10.3389/fimmu.2021.691715.
39. Tortorici, M.A., Czudnochowski, N., Starr, T.N., Marzi, R., Walls, A.C., Zatta, F., Bowen, J.E., Jaconi, S., Di Iulio, J., Wang, Z., et al. (2021). Broad sarbecovirus neutralization by a human monoclonal antibody. Nature *597*, 103-108. 10.1038/s41586-021-03817-4.
40. Wec, A.Z., Wrapp, D., Herbert, A.S., Maurer, D.P., Haslwanter, D., Sakharkar, M., Jangra, R.K., Dieterle, M.E., Lilov, A., Huang, D., et al. (2020). Broad neutralization of SARS-related viruses by human monoclonal antibodies. Science *369*, 731-736. 10.1126/science.abc7424.
41. Andrabi, R., Pallesen, J., Allen, J.D., Song, G., Zhang, J., de Val, N., Gegg, G., Porter, K., Su, C.Y., Pauthner, M., et al. (2019). The Chimpanzee SIV Envelope Trimer:

574 Structure and Deployment as an HIV Vaccine Template. Cell reports *27*, 2426-2441
575 e2426. 10.1016/j.celrep.2019.04.082.
576 42. Letko, M., Marzi, A., and Munster, V. (2020). Functional assessment of cell entry and
577 receptor usage for SARS-CoV-2 and other lineage B betacoronaviruses. Nat Microbiol *5*,
578 562-569. 10.1038/s41564-020-0688-y.
579 43. Menachery, V.D., Yount, B.L., Jr., Sims, A.C., Debbink, K., Agnihothram, S.S., Gralinski,
580 L.E., Graham, R.L., Scobey, T., Plante, J.A., Royal, S.R., et al. (2016). SARS-like WIV1-
581 CoV poised for human emergence. Proceedings of the National Academy of Sciences of
582 the United States of America *113*, 3048-3053. 10.1073/pnas.1517719113.
583 44. Feldman, J., Bals, J., Altomare, C.G., St Denis, K., Lam, E.C., Hauser, B.M., Ronsard,
584 L., Sangesland, M., Moreno, T.B., Okonkwo, V., et al. (2021). Naive human B cells
585 engage the receptor binding domain of SARS-CoV-2, variants of concern, and related
586 sarbecoviruses. Sci Immunol *6*, eabl5842. 10.1126/sciimmunol.abl5842.
587 45. Collier, A.-r.Y., Miller, J., Hachmann, N.P., McMahan, K., Liu, J., Bondzie, E.A., Gallup,
588 L., Rowe, M., Schonberg, E., Thai, S., et al. (2023). Immunogenicity of BA.5 Bivalent
589 mRNA Vaccine Boosters. New England Journal of Medicine *388*, 565-567.
590 10.1056/NEJMc2213948.
591 46. Chalkias, S., Harper, C., Vrbicky, K., Walsh, S.R., Essink, B., Brosz, A., McGhee, N.,
592 Tomassini, J.E., Chen, X., Chang, Y., et al. (2022). A Bivalent Omicron-Containing
593 Booster Vaccine against Covid-19. New England Journal of Medicine *387*, 1279-1291.
594 10.1056/NEJMoa2208343.
595 47. Cohen, A.A., Gnanapragasam, P.N.P., Lee, Y.E., Hoffman, P.R., Ou, S., Kakutani, L.M.,
596 Keeffe, J.R., Wu, H.J., Howarth, M., West, A.P., et al. (2021). Mosaic nanoparticles elicit
597 cross-reactive immune responses to zoonotic coronaviruses in mice. Science.
598 10.1126/science.abf6840.
599 48. Liu, H., Kaku, C.I., Song, G., Yuan, M., Andrabi, R., Burton, D.R., Walker, L.M., and
600 Wilson, I.A. (2022). Human antibodies to SARS-CoV-2 with a recurring YYDRxG motif
601 retain binding and neutralization to variants of concern including Omicron. Commun Biol
602 *5*, 766. 10.1038/s42003-022-03700-6.
603 49. Liu, L., Iketani, S., Guo, Y., Reddem, E.R., Casner, R.G., Nair, M.S., Yu, J., Chan, J.F.-
604 W., Wang, M., Cerutti, G., et al. (2022). An antibody class with a common CDRH3 motif
605 broadly neutralizes sarbecoviruses. Science translational medicine *14*, eabn6859.
606 doi:10.1126/scitranslmed.abn6859.
607 50. Gaebler, C., Wang, Z., Lorenzi, J.C.C., Muecksch, F., Finkin, S., Tokuyama, M., Cho, A.,
608 Jankovic, M., Schaefer-Babajew, D., Oliveira, T.Y., et al. (2021). Evolution of antibody
609 immunity to SARS-CoV-2. Nature *591*, 639-644. 10.1038/s41586-021-03207-w.
610 51. Cho, A., Muecksch, F., Schaefer-Babajew, D., Wang, Z., Finkin, S., Gaebler, C., Ramos,
611 V., Cipolla, M., Mendoza, P., Agudelo, M., et al. (2021). Anti-SARS-CoV-2 receptor-
612 binding domain antibody evolution after mRNA vaccination. Nature *600*, 517-522.
613 10.1038/s41586-021-04060-7.
614 52. Dejnirattisai, W., Zhou, D., Ginn, H.M., Duyvesteyn, H.M.E., Supasa, P., Case, J.B.,
615 Zhao, Y., Walter, T.S., Mentzer, A.J., Liu, C., et al. (2021). The antigenic anatomy of
616 SARS-CoV-2 receptor binding domain. Cell *184*, 2183-2200.e2122.
617 10.1016/j.cell.2021.02.032.
618 53. Reincke, S.M., Yuan, M., Kornau, H.C., Corman, V.M., van Hoof, S., Sánchez-Sendin,
619 E., Ramberger, M., Yu, W., Hua, Y., Tien, H., et al. (2022). SARS-CoV-2 Beta variant
620 infection elicits potent lineage-specific and cross-reactive antibodies. Science *375*, 782-
621 787. 10.1126/science.abm5835.
622 54. Dacon, C., Peng, L., Lin, T.-H., Tucker, C., Lee, C.-C.D., Cong, Y., Wang, L., Purser, L.,
623 Cooper, A.J.R., Williams, J.K., et al. (2022). Rare, convergent antibodies targeting the

stem helix broadly neutralize diverse betacoronaviruses. Cell host & microbe. https://doi.org/10.1016/j.chom.2022.10.010.

55. Zhou, P., Song, G., Liu, H., Yuan, M., He, W.-t., Beutler, N., Zhu, X., Tse, L.V., Martinez, D.R., Schäfer, A., et al. (2023). Broadly neutralizing anti-S2 antibodies protect against all three human betacoronaviruses that cause deadly disease. Immunity. 10.1016/j.immuni.2023.02.005.

56. Ye, J., Ma, N., Madden, T.L., and Ostell, J.M. (2013). IgBLAST: an immunoglobulin variable domain sequence analysis tool. Nucleic acids research *41*, W34-W40. 10.1093/nar/gkt382.

57. Andrabi, R., Bhiman, J.N., and Burton, D.R. (2018). Strategies for a multi-stage neutralizing antibody-based HIV vaccine. Curr Opin Immunol *53*, 143-151. 10.1016/j.coi.2018.04.025.

58. Andrabi, R., Voss, J.E., Liang, C.H., Briney, B., McCoy, L.E., Wu, C.Y., Wong, C.H., Poignard, P., and Burton, D.R. (2015). Identification of Common Features in Prototype Broadly Neutralizing Antibodies to HIV Envelope V2 Apex to Facilitate Vaccine Design. Immunity *43*, 959-973. 10.1016/j.immuni.2015.10.014.

59. Steichen, J.M., Lin, Y.C., Havenar-Daughton, C., Pecetta, S., Ozorowski, G., Willis, J.R., Toy, L., Sok, D., Liguori, A., Kratochvil, S., et al. (2019). A generalized HIV vaccine design strategy for priming of broadly neutralizing antibody responses. Science *366*. 10.1126/science.aax4380.

60. Willis, J.R., Berndsen, Z.T., Ma, K.M., Steichen, J.M., Schiffner, T., Landais, E., Liguori, A., Kalyuzhniy, O., Allen, J.D., Baboo, S., et al. (2022). Human immunoglobulin repertoire analysis guides design of vaccine priming immunogens targeting HIV V2-apex broadly neutralizing antibody precursors. Immunity *55*, 2149-2167.e2149. 10.1016/j.immuni.2022.09.001.

61. Gorman, J., Soto, C., Yang, M.M., Davenport, T.M., Guttman, M., Bailer, R.T., Chambers, M., Chuang, G.Y., DeKosky, B.J., Doria-Rose, N.A., et al. (2016). Structures of HIV-1 Env V1V2 with broadly neutralizing antibodies reveal commonalities that enable vaccine design. Nature structural & molecular biology *23*, 81-90. 10.1038/nsmb.3144.

62. Zhan, W., Tian, X., Zhang, X., Xing, S., Song, W., Liu, Q., Hao, A., Hu, Y., Zhang, M., Ying, T., et al. (2022). Structural Study of SARS-CoV-2 Antibodies Identifies a Broad-Spectrum Antibody That Neutralizes the Omicron Variant by Disassembling the Spike Trimer. Journal of virology *96*, e0048022. 10.1128/jvi.00480-22.

63. Wang, S., Sun, H., Zhang, Y., Yuan, L., Wang, Y., Zhang, T., Wang, S., Zhang, J., Yu, H., Xiong, H., et al. (2022). Three SARS-CoV-2 antibodies provide broad and synergistic neutralization against variants of concern, including Omicron. Cell reports *39*, 110862. 10.1016/j.celrep.2022.110862.

64. Hurlburt, N.K., Homad, L.J., Sinha, I., Jennewein, M.F., MacCamy, A.J., Wan, Y.H., Boonyaratanakornkit, J., Sholukh, A.M., Jackson, A.M., Zhou, P., et al. (2022). Structural definition of a pan-sarbecovirus neutralizing epitope on the spike S2 subunit. Commun Biol *5*, 342. 10.1038/s42003-022-03262-7.

65. Pinto, D., Sauer, M.M., Czudnochowski, N., Low, J.S., Tortorici, M.A., Housley, M.P., Noack, J., Walls, A.C., Bowen, J.E., Guarino, B., et al. (2021). Broad betacoronavirus neutralization by a stem helix-specific human antibody. Science *373*, 1109-1116. 10.1126/science.abj3321.

66. Zhou, P., Yuan, M., Song, G., Beutler, N., Shaabani, N., Huang, D., He, W.-t., Zhu, X., Callaghan, S., Yong, P., et al. (2022). A human antibody reveals a conserved site on beta-coronavirus spike proteins and confers protection against SARS-CoV-2 infection. Science translational medicine *0*, eabi9215. doi:10.1126/scitranslmed.abi9215.

67. Dacon, C., Tucker, C., Peng, L., Lee, C.D., Lin, T.H., Yuan, M., Cong, Y., Wang, L., Purser, L., Williams, J.K., et al. (2022). Broadly neutralizing antibodies target the coronavirus fusion peptide. Science *377*, 728-735. 10.1126/science.abq3773.
68. Sun, X., Yi, C., Zhu, Y., Ding, L., Xia, S., Chen, X., Liu, M., Gu, C., Lu, X., Fu, Y., et al. (2022). Neutralization mechanism of a human antibody with pan-coronavirus reactivity including SARS-CoV-2. Nat Microbiol *7*, 1063-1074. 10.1038/s41564-022-01155-3.
69. Low, J.S., Jerak, J., Tortorici, M.A., McCallum, M., Pinto, D., Cassotta, A., Foglierini, M., Mele, F., Abdelnabi, R., Weynand, B., et al. (2022). ACE2-binding exposes the SARS-CoV-2 fusion peptide to broadly neutralizing coronavirus antibodies. Science *377*, 735-742. 10.1126/science.abq2679.
70. Sequences of 22 Sarbecoviruses including SARS-CoV-2, SARS-CoV and SARS-related coronaviruses (SARSr-CoVs) were used for this analysis: NCBI Reference Sequence YP_009724390.1 (SARS-CoV-2) and variants Alpha, Beta, Gamma, Delta, Omicron BA.1, BA.2, BA.5, BQ.1.1, and XBB.1.5, GenBank ABF65836.1 (SARS-CoV), GenBank ALK02457.1 (Bat SARSr-CoV WIV16), GenBank AGZ48828.1 (Bat SARSr-CoV WIV1), GenBank ACU31032.1 (Bat SARSr-CoV Rs672), GenBank AIA62320.1 (Bat SARSr-CoV GX2013), GenBank AAZ67052.1 (Bat SARSr-CoV Rp3), GenBank AIA62300.1 (Bat SARSr-CoV SX2013), GenBank ABD75323.1 (Bat SARSr-CoV Rf1), GenBank AIA62310.1 (Bat SARSr-CoV HuB2013), GenBank AAY88866.1 (Bat SARSr-CoV HKU3-1), GenBank AID16716.1 (Bat SARSr-CoV Longquan-140), GenBank AVP78031.1 (Bat SARSr-CoV ZC45), GenBank AVP78042.1 (Bat SARSr-CoV ZXC21), GenBank QHR63300.2 (Bat CoV RaTG13), NCBI Reference Sequence YP_003858584.1 (Bat SARSr-CoV BM48-31), GISAID EPI_ISL_410721 (Pangolin-CoV Guandong2019), GenBank QIA48632.1 (Pangolin-CoV Guangxi), GenBank AGZ48806.1 (Bat SARSr-CoV RsSHC0144), GenBank ATO98120.1 (Bat SARSr-CoV Rs4081), GenBank AGC74176.1 (Bat SARSr-CoV Yun11), GenBank APO40579.1 (Bat SARSr-CoV BtKY72).
71. Walls, A.C., Park, Y.-J., Tortorici, M.A., Wall, A., McGuire, A.T., and Veesler, D. (2020). Structure, Function, and Antigenicity of the SARS-CoV-2 Spike Glycoprotein. Cell *181*, 281-292.e286. 10.1016/j.cell.2020.02.058.
72. Lv, H., Wu, N.C., Tsang, O.T., Yuan, M., Perera, R., Leung, W.S., So, R.T.Y., Chan, J.M.C., Yip, G.K., Chik, T.S.H., et al. (2020). Cross-reactive Antibody Response between SARS-CoV-2 and SARS-CoV Infections. Cell reports *31*, 107725. 10.1016/j.celrep.2020.107725.
73. Liu, H., Wu, N.C., Yuan, M., Bangaru, S., Torres, J.L., Caniels, T.G., van Schooten, J., Zhu, X., Lee, C.D., Brouwer, P.J.M., et al. (2020). Cross-Neutralization of a SARS-CoV-2 Antibody to a Functionally Conserved Site Is Mediated by Avidity. Immunity *53*, 1272-1280.e1275. 10.1016/j.immuni.2020.10.023.
74. Ekiert, D.C., Friesen, R.H., Bhabha, G., Kwaks, T., Jongeneelen, M., Yu, W., Ophorst, C., Cox, F., Korse, H.J., Brandenburg, B., et al. (2011). A highly conserved neutralizing epitope on group 2 influenza A viruses. Science *333*, 843-850. 10.1126/science.1204839.
75. Bailey, L.J., Sheehy, K.M., Dominik, P.K., Liang, W.G., Rui, H., Clark, M., Jaskolowski, M., Kim, Y., Deneka, D., Tang, W.J., and Kossiakoff, A.A. (2018). Locking the Elbow: Improved Antibody Fab Fragments as Chaperones for Structure Determination. Journal of molecular biology *430*, 337-347. 10.1016/j.jmb.2017.12.012.
76. Lieu, R., Antonysamy, S., Druzina, Z., Ho, C., Kang, N.R., Pustilnik, A., Wang, J., and Atwell, S. (2020). Rapid and robust antibody Fab fragment crystallization utilizing edge-to-edge beta-sheet packing. PloS one *15*, e0232311. 10.1371/journal.pone.0232311.

77. Vonrhein, C., Flensburg, C., Keller, P., Sharff, A., Smart, O., Paciorek, W., Womack, T., and Bricogne, G. (2011). Data processing and analysis with the autoPROC toolbox. Acta Crystallogr D Biol Crystallogr *67*, 293-302. 10.1107/s0907444911007773.
78. McCoy, A.J., Grosse-Kunstleve, R.W., Adams, P.D., Winn, M.D., Storoni, L.C., and Read, R.J. (2007). Phaser crystallographic software. J Appl Crystallogr *40*, 658-674. 10.1107/s0021889807021206.
79. Emsley, P., Lohkamp, B., Scott, W.G., and Cowtan, K. (2010). Features and development of Coot. Acta Crystallogr D Biol Crystallogr *66*, 486-501. 10.1107/s0907444910007493.
80. Adams, P.D., Afonine, P.V., Bunkóczi, G., Chen, V.B., Davis, I.W., Echols, N., Headd, J.J., Hung, L.W., Kapral, G.J., Grosse-Kunstleve, R.W., et al. (2010). PHENIX: a comprehensive Python-based system for macromolecular structure solution. Acta Crystallogr D Biol Crystallogr *66*, 213-221. 10.1107/s0907444909052925.
81. Krissinel, E., and Henrick, K. (2007). Inference of macromolecular assemblies from crystalline state. Journal of molecular biology *372*, 774-797. 10.1016/j.jmb.2007.05.022.
82. Scheres, S.H. (2012). RELION: implementation of a Bayesian approach to cryo-EM structure determination. J Struct Biol *180*, 519-530. 10.1016/j.jsb.2012.09.006.
83. Pettersen, E.F., Goddard, T.D., Huang, C.C., Meng, E.C., Couch, G.S., Croll, T.I., Morris, J.H., and Ferrin, T.E. (2021). UCSF ChimeraX: Structure visualization for researchers, educators, and developers. Protein Science *30*, 70-82. https://doi.org/10.1002/pro.3943.
84. Chen, V.B., Arendall, W.B., 3rd, Headd, J.J., Keedy, D.A., Immormino, R.M., Kapral, G.J., Murray, L.W., Richardson, J.S., and Richardson, D.C. (2010). MolProbity: all-atom structure validation for macromolecular crystallography. Acta Crystallogr D Biol Crystallogr *66*, 12-21. 10.1107/s0907444909042073.

Acknowledgements

This work was supported by National Institutes of Health-(NIH), National Institute of Allergy and Infectious Diseases-(NIAID) awards, R01AI170928 (R.A.) and CHAVD UM1 AI44462 (D.R.B.) and the Bill and Melinda Gates Foundation INV-004923 (I.A.W., D.R.B.). We thank Henry Tien for technical support with the crystallization robot, and Wenli Yu for protein production. We are grateful to the staff of the Stanford Synchrotron Radiation Lightsource (SSRL) beamlines 12-1 and Advanced Photon Source (APS) beamline 23-ID-B and 23-ID-D for assistance. This research used resources of the SSRL, SLAC National Accelerator Laboratory, which is supported by the U.S. Department of Energy, Office of Science, Office of Basic Energy Sciences under Contract No. DE-AC02–76SF00515. The SSRL Structural Molecular Biology Program is supported by the DOE Office of Biological and Environmental Research, and by the National Institutes of Health, National Institute of General Medical Sciences (including P41GM103393). This research also used resources of the Advanced Photon Source, a U.S. Department of Energy (DOE) Office of Science User Facility, operated for the DOE Office of Science by Argonne National Laboratory under Contract No. DE-AC02-06CH11357. Extraordinary facility operations were supported in part by the DOE Office of Science through the National Virtual Biotechnology Laboratory, a consortium of DOE national laboratories focused on the response to COVID-19, with funding provided by the Coronavirus CARES Act.

Author contributions

G.S., M.Y., H.L., T.C., D.R.B., I.A.W. and R.A. conceived and designed the study. G.S., T.C., W.H., R.M., K.D., P.Z., S.C., N.M., P.Y., F.A., G.A., A.L.V., X.L., M.M. and L.P. performed BLI, virus preparation, neutralization, and characterization of monoclonal antibodies. Y.S. and B.B performed immunogenetic analysis of antibodies. M.Y., H.L., and Z.F. crystallized the antibody-antigen complexes and determined the crystal structures. M.Y. and H.L., collected X-ray data. M.Y., H.L., X.Z. and I.A.W. analyzed the structural data. R.N.L. and J.L.T. conducted the negative stain electron microscopy studies. G.S., M.Y., H.L., T.C., R.N.L., J.L.T., W.H., R.M., K.D., P.Z., S.C., N.M., P.Y., F.A., G.A., A.L.V., X.L., M.M., Z.F., X.Z., L.P., D.N., Y.S., B.B., A.B.W., D.R.B., I.A.W. and R.A. designed the experiments and/or analyzed the data. G.S., M.Y., H.L., T.C., D.R.B., I.A.W. and R.A. wrote the paper, and all authors reviewed and edited the paper.

Declaration of interests

G.S., W.H., P.Z., S.C., R.M., K.D., D.R.B. and R.A. are listed as inventors on pending patent applications describing the betacoronavirus broadly neutralizing antibodies. All other authors have no competing interests to declare.

Key Resource Table

REAGENT or RESOURCE	SOURCE	IDENTIFIER
Chemicals, Peptides, and Recombinant Proteins		
NEBuilder® HiFi DNA Assembly Master Mix	New England Biolabs	#E2621L
40 K polyethylenimine (PEI)	Polysciences	#24765-1
FectoPRO	Polyplus	#116-001

Lipofectamine 2000	ThermoFisher Scientific	#11668019
Valproic acid sodium salt	Sigma	# P4543-100G
45% D-(+)-Glucose Solution	Sigma	# G8769-100ML
L-glutamine	Corning	# 25-005-CI
Penicillin-streptomycin	Corning	# 30-002-CI
DEAE-dextran	Sigma-Aldrich	# 93556-1G
SARS-CoV-2 and VOCs spike and RBD proteins	In house	N/A
SARS-CoV-1, YN02, BM4831 spike and RBD proteins	In house	N/A
Bright-Glo Luciferase Assay System	Promega	#E2620
Papain	Sigma-Aldrich	#P3125
Deposited Data		
Structure of CC25.36 + SARS-CoV-2 RBD complex	RCSB PDB	8SIQ
Structure of CC25.54 + SARS-CoV-2 RBD complex	RCSB PDB	8SIR
Structure of CC84.2 + SARS-CoV-2 RBD complex	RCSB PDB	8SIS
Structure of CC84.24 + SARS-CoV-2 RBD complex	RCSB PDB	8SIT
Structure of CC25.4 + SARS-CoV-2 RBD complex	RCSB PDB	8SDF
Structure of CC25.43 + SARS-CoV-2 RBD complex	RCSB PDB	8SDG
Structure of CC25.56 + SARS-CoV-2 RBD complex	RCSB PDB	8SDH
Experimental Models: Cell Lines		
FreeStyle293-F cells	Thermo Fisher Scientific	#R79007
Expi293F cells	Gibco	#A14527
293T cells	ATCC	# CRL-3216
HeLa-ACE2 cells	In house	N/A
Recombinant DNA		
phCMV3	Genlantis	#P003300
pBOB-hACE2	In house	N/A
SARS-CoV-2 6P Mut7	In House	N/A
Software and Algorithms		
V-Quest online tool	IMGT	http://www.imgt.org
Prism 8	GraphPad	https://www.graphpad.com/scientific-software/prism/
ForteBio Data Analysis software	Sartorius	https://www.sartorius.com/en
PyMOL V2.4.2	PyMOL by Schrödinger	https://pymol.org
HKL2000	DOI: 10.1016/S0076-6879(97)76066-X	N/A

AutoPROC	DOI: 10.1107/S0907444911007773	N/A
Phaser	DOI: 10.1107/S0021889807021206	N/A
Coot	DOI: 10.1107/S0907444910007493	N/A
MolProbity	DOI: 10.1107/S0907444909042073	N/A
RELION 3.1	SciLifeLab	https://relion.readthedocs.io/en/release-4.0/
EPU	Thermo Fisher	https://www.thermofisher.com/us/en/home/electron-microscopy/products/software-em-3d-vis/epu-software.html
ChimeraX	UCSF	https://www.rbvi.ucsf.edu/chimerax/
Other		
FreeStyle293 Expression Medium	Gibco	#12338018
Expi293 Expression Medium	Gibco	#A1435101
DMEM	Corning	#10-017-CV
FBS	Omega Scientific	#NC0471611
Transfectagro™	Corning	#40-300-CV
Opti-MEM™	Thermo Fisher Scientific	#31985070
0.2 um membrane filters	Fisher Scientific	#564-0020
Steriflip™ Vacuum Filter Units	MilliporeSigma	#SCGP00525
HisPur Ni-NTA Resin	Thermo Fisher Scientific	#88221
Superdex 200 Increase10/300 GL column	GE Healthcare	#GE28-9909-44
Praesto Protein A Affinity Chromatography Resin	Purolite	# PR00300-164
Protein G Sepharose	GE Healthcare	#45000118
Econo-Pac columns	BioRad	#7321010
StrepTactin XT 4FLOW	IBA Life Sciences	#2-5010-025
Amicon tubes (100K, 30K, 10K)	Millipore	#UFC9100, #UFC9030, #UFC9010
Bio-One Polypropylene 96-well F-Bottom Microplates	Greiner	#655209
Anti-human IgG Fc capture (AHC) biosensors	ForteBio	#18-5060
96 Half Area Well Solid White Flat Bottom Polystyrene TC-treated Microplates	Corning	#3688

Pierce™ Fab Preparation Kit	Thermo Fisher	#44985

Resource Availability

Lead contact

Further information and requests for resources and reagents should be directed to and will be fulfilled by the lead contact, Raiees Andrabi (andrabi@scripps.edu)

Materials availability

Upon specific request and execution of a material transfer agreement (MTA) from The Scripps Research Institute to the Lead Contact, Antibody plasmids will be made available.

Data and code availability

The data supporting the findings of this study are available within the published article and summarized in the corresponding tables, figures, and supplemental materials. Inferred germline antibody sequences have been deposited in GenBank under accession numbers XXXX-XXXX. X-ray coordinates and structure factors have been deposited in the RCSB Protein Data Bank under accession codes 8SIQ, 8SIR, 8SIS, 8SIT, 8SDF, 8SDG, and 8SDH.

Figures and legends

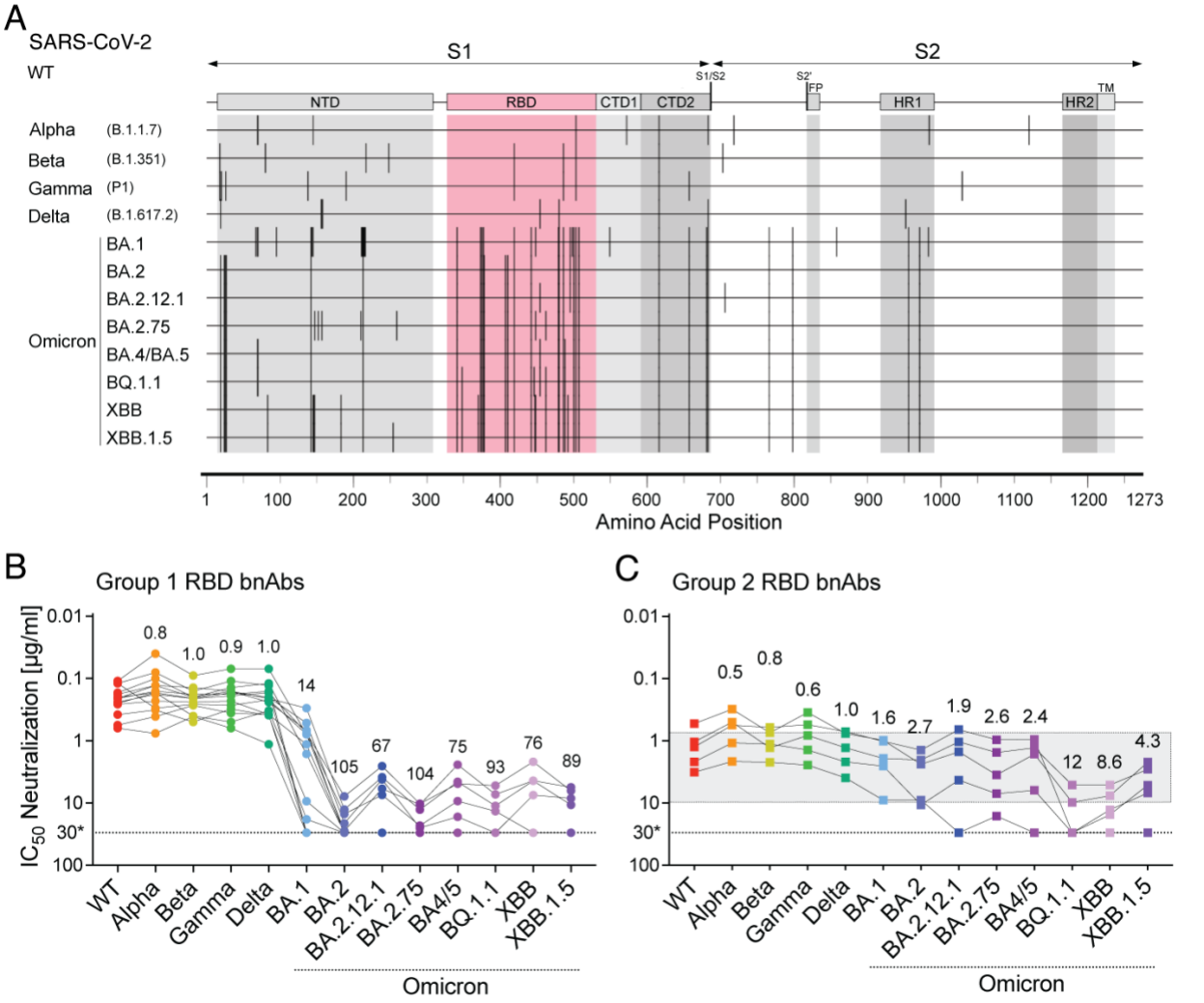

Figure 1. Neutralization of SARS-CoV-2 variants by RBD human broadly neutralizing antibodies.

A. Schematic showing amino acid sequence alignment of SARS-CoV-2 spike region across 12 VOCs including Alpha (B.1.1.7), Beta (B.1.351), Gamma (P.1), Delta (B.1.617.2), Omicron subvariants BA.1, BA.2, BA.2.12.1, BA.2.75, BA.4/BA.5, BQ.1.1, XBB, and XBB.1.5. Vertical lines indicated mismatches compared to SARS-CoV-2 WT (Wuhan). Amino acid positions are illustrated at the bottom, S1 and S2 subunits are shown by arrowed lines at the top. Different domains are indicated (NTD, N-terminal domain; RBD, receptor-binding domain; CTD1, C-terminal domain 1; CTD2, C-terminal domain 2; S1/S2, S1/S2 furin cleavage site; S2′, S2′ TMPRSS2 or cathepsin B/L cleavage site; FP, fusion peptide; HR1, heptad repeat 1; HR2, heptad repeat 2; TM, transmembrane anchor), with the RBD region highlighted in red, containing the majority of the mutations.

B-C. Neutralization IC_{50} of RBD bnAbs from group 1 (**B**) and group 2 (**C**) for the panel of SARS-CoV-2 WT and variants. Each variant is indicated by a different color. Round data points represent group 1 RBD bnAbs, square data points represent group 2 RBD bnAbs.

827 The dotted line shows the limit of antibody dilution (30µg/ml). Values above each column
828 indicate fold change of IC_{50}s against each variant in comparison with WT. The grey
829 shaded area highlights the bnAbs in group 2 showing relatively consistent neutralization
830 IC_{50} across SARS-CoV-2 WT and variants.
831

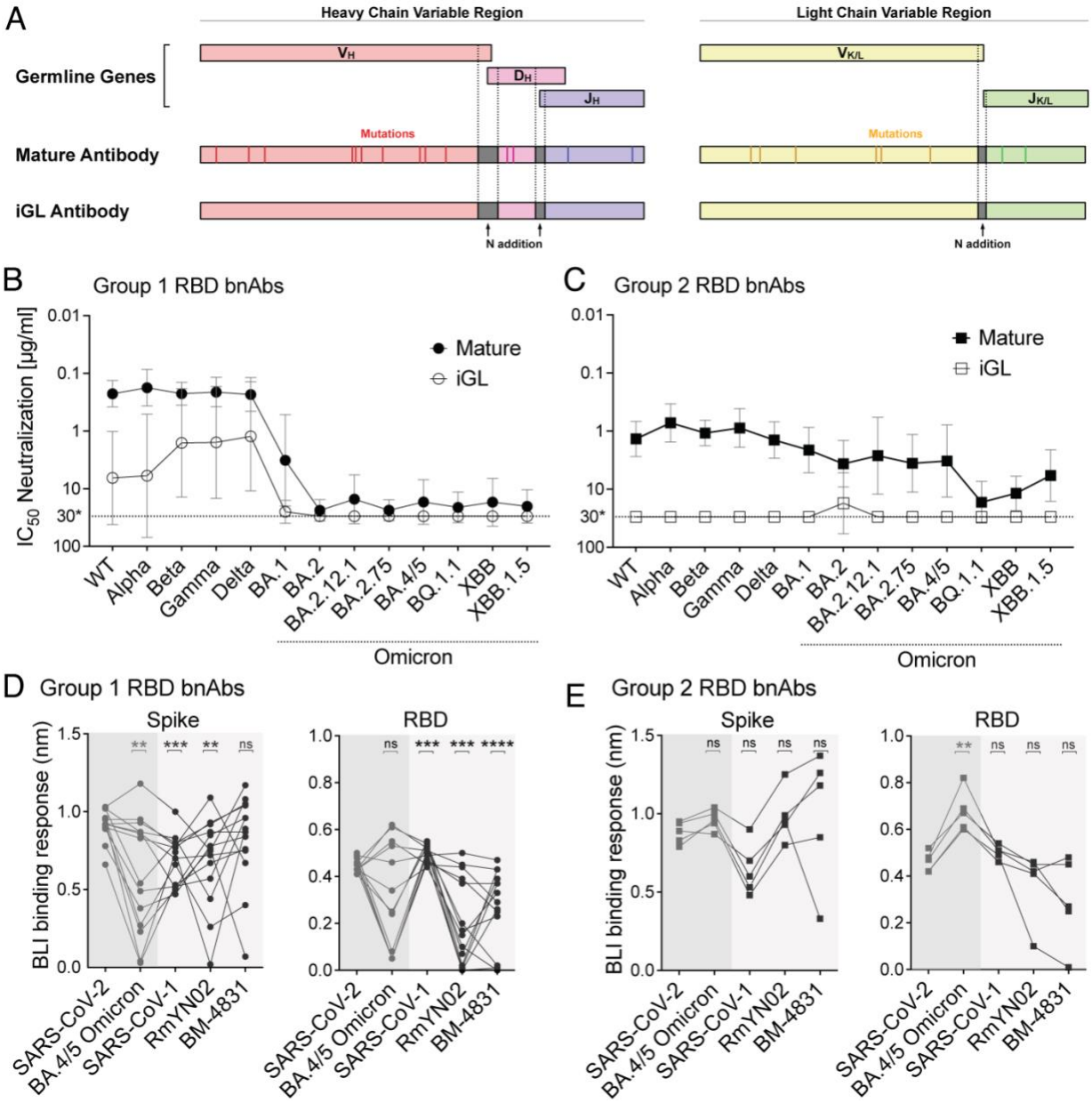

Figure 2. Neutralization and binding of mature RBD bnAbs and their inferred germline (iGL) versions against SARS-CoV-2 VOCs and other sarbecoviruses.

A. Schematic showing design of inferred germline versions of bnAbs based on mature antibody heavy chain (left) and light chain (right) variable region sequences. The V/D/J genes of heavy chains (V_H, D_H, J_H) and V/J genes of kappa or lambda light chains ($V_{K/L}$, $J_{K/L}$) were reverted to their corresponding germlines (IMGT/V-QUEST tool). The mutations represented by vertical lines were eliminated in the inferred germline antibody sequences. The non-templated N additions between V(/D)/J, indicated as dark grey, remained the same as in the mature antibody.

B-C. Average neutralization IC_{50} values of all group 1 (B) and group 2 (C) RBD bnAbs comparing the mature antibody (bold) to their inferred germ line versions (open) tested with pseudotyped versions of SARS-CoV-2 WT (Wuhan) and 12 VOCs including Alpha (B.1.1.7), Beta (B.1.351), Gamma (P.1), Delta (B.1.617.2), Omicron subvariants BA.1,

BA.2, BA.2.12.1, BA.2.75, BA.4/5, BQ.1.1, XBB, and XBB.1.5. Round data points represent group 1 RBD bnAbs, square data points represented group 2 RBD bnAbs. Each data point represents the geometric mean ± geometric SD of neutralization IC_{50} for specific variants by all bnAbs within the corresponding group (n = 14 for group 1, n = 5 for group 2).

D-E. BLI binding response (nm) of group 1 (D) and group 2 (E) RBD bnAbs to the trimeric stabilized spike proteins and monomeric RBD proteins of SARS-CoV-2 (Wuhan and BA.4/5), clade 1b SARS-CoV-1, clade 2 RmYN02, and clade 3 BM-4831 sarbecoviruses. Statistical comparisons between groups were performed using a two-tailed Mann-Whitney U-test (ns: $p > 0.05$, *: $p < 0.05$, **: $p < 0.005$, ***: $p < 0.001$, ****: $p < 0.0001$).

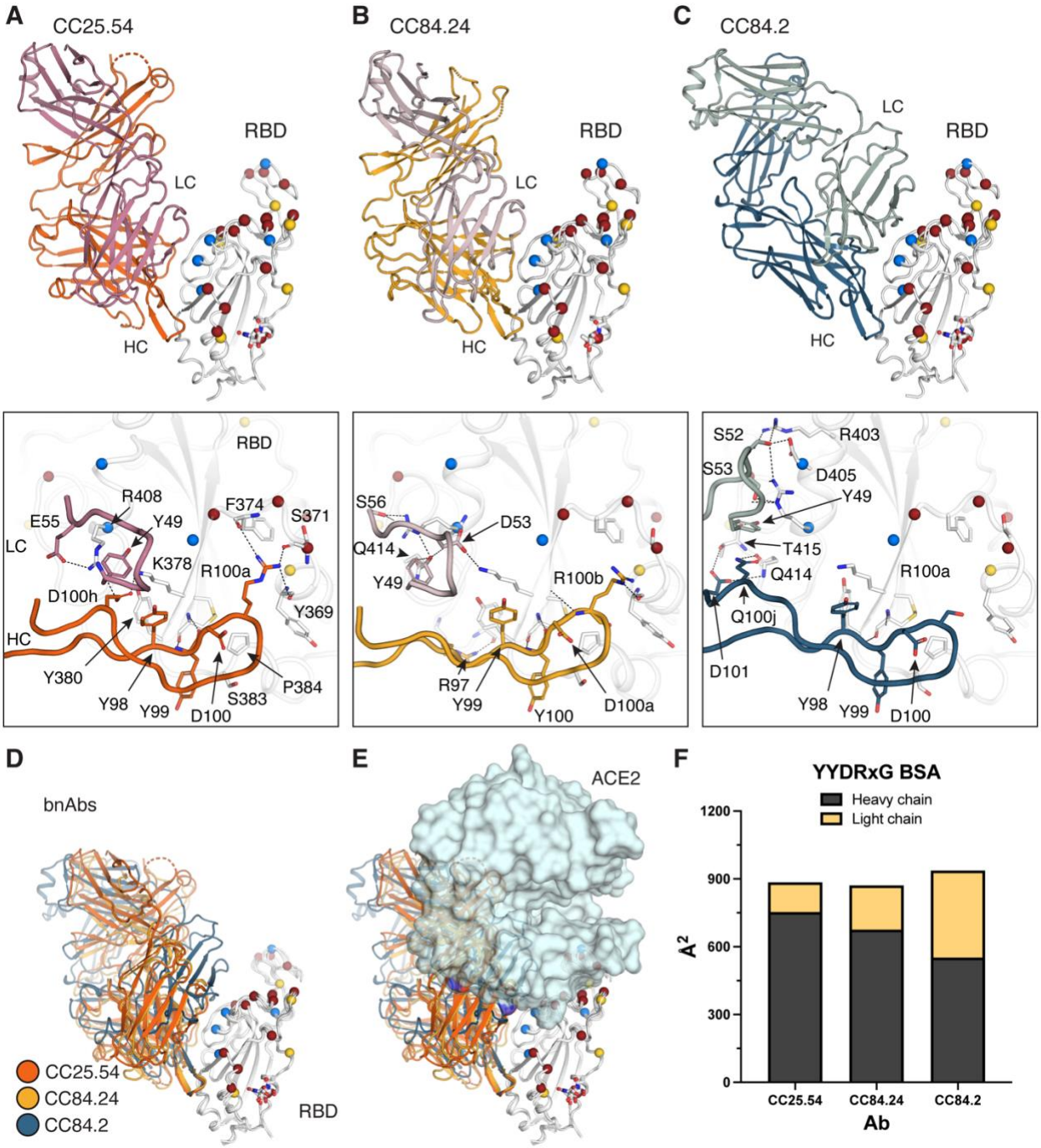

Figure 3. Crystal structures of representative YYDRxG antibodies from group 1 bnAbs. X-ray structures of two YYDRxG antibodies, CC25.54 (**A**) and CC84.24 (**B**), and a YYDSSG (YYDRxG precursor) antibody CC84.2 (**C**) are shown in ribbon representation (sticks represents observed N343 glycans in SARS-CoV-2 RBD crystal structure). The same perspective view is used for easy comparison. The CC25.54 heavy chain is colored in orange, light chain in rose pink; CC84.24 heavy chain in yellow, light chain in violet; CC84.2 heavy chain in navy blue, and light chain in teal. Residues from CDRH2 and H3 that interact with the RBD are shown in sticks. Dashed lines represent polar interactions. RBD residues that are mutated in Omicron are shown

as spheres. Red represents residues mutated in BA.1, and additional mutations in blue in BA.4/5 and yellow in XBB.1.5. (**D**) Overlay comparison of YYDRxG antibodies determined in this study. Crystal structures are superimposed on SARS-CoV-2 RBD to compare the approach angles of these antibodies. (**E**) YYDRxG antibodies clash with ACE2 binding, although their epitope footprints do not overlap. Composite structures of YYDRxG antibodies from this study and ACE2 in complex with SARS-CoV-2 RBD (PDB ID: 6M0J) were used for comparison. (**F**) Comparison of the buried surface area (BSA) on SARS-CoV-2 RBD from the heavy and light chains of YYDRxG antibodies.

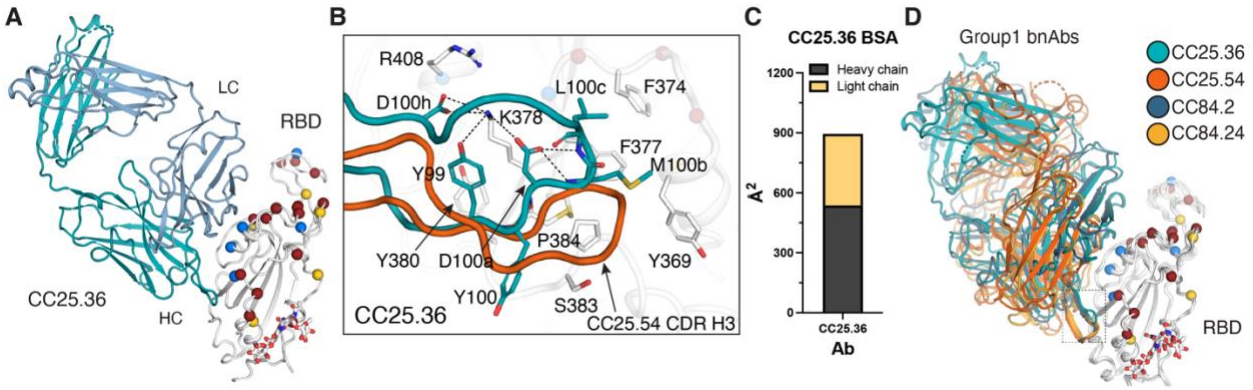

Figure 4. Crystal structure of group 1 antibody CC25.36 in complex with SARS-CoV-2 RBD. Heavy chain is colored in turquoise blue, and light chain in baby blue. RBD residues that are mutated in Omicron are shown as spheres. Red represents those mutated in BA.1; blue, additional mutations in BA.4/5; yellow, additional mutations in XBB.1.5.

A. Overall structure of CC25.36 is shown in ribbon representation. Sticks represent glycans at N343 in SARS-CoV-2 RBD.

B. Interactions between CDRH3 and RBD. Residues involved in the antibody-antigen interface are shown in sticks. The same perspective view as Figure 3A was used. CC25.54 CDR H3 was superimposed for easy comparison with Fig. 3 in orange.

C. BSA on SARS-CoV-2 RBD from the CC25.36 heavy and light chains.

D. CC25.36 CDRH3 uses a distinct binding mode. Structures of CC25.36 and YYDRxG antibodies determined in this study are superimposed on the RBD. CC25.36 CDR H3 (boxed) binds the same site as YYDRxG antibodies but with a different binding mode, although they use similar approach angles that can compete with ACE2.

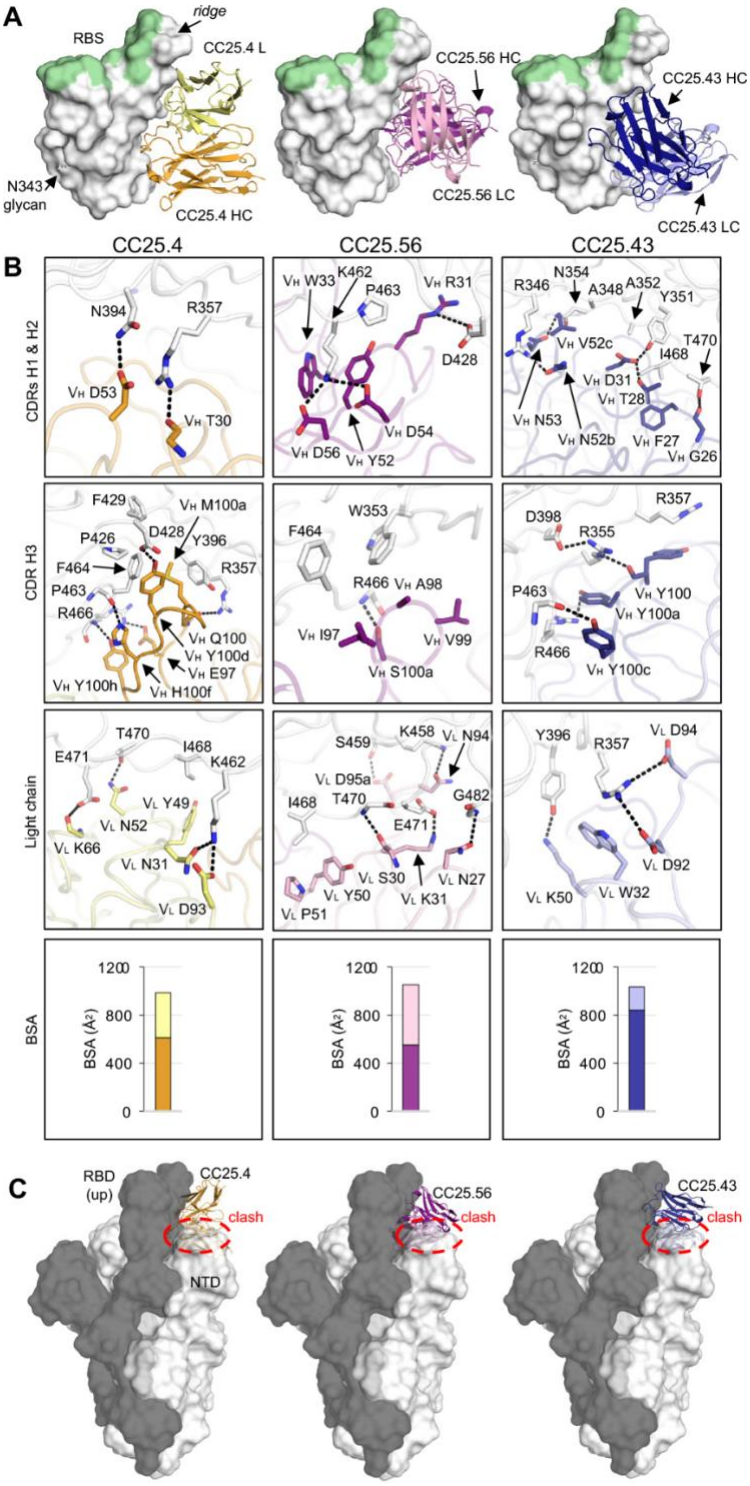

Figure 5. Crystal structures of SARS-CoV-2 RBD in complex with site V antibodies. The SARS-CoV-2 RBD is shown in white, while the receptor binding site (RBS) is highlighted in pale green throughout all the figures. For clarity, only the variable domains of the antibodies are shown in all figures.

A. Crystal structures of SARS-CoV-2 RBD in complex with site V antibodies. The RBD-N343 N-glycan is shown as sticks. Heavy and light chains of CC25.4 are in orange and

yellow, while those of CC25.56 in dark and light pink, and CC25.43 in dark and light blue, respectively.
B. Detailed interactions between SARS-CoV-2 RBD and the antibodies. Hydrogen bonds and salt bridges are indicated by dashed lines. Surface area of SARS-CoV-2 buried by heavy and light chains of each antibody are shown in the bottom panels.
C. Models of antibody/RBD structures superimposed onto SARS-CoV-2 spike structures with one-up RBD (PDB 7KJ5). The spike protomer with an up-RBD is shown in grey, while the other two protomers are shown in white. Binding to up-RBDs, site V antibodies would clash with the NTD of the adjacent protomer (indicated with red circles).

A

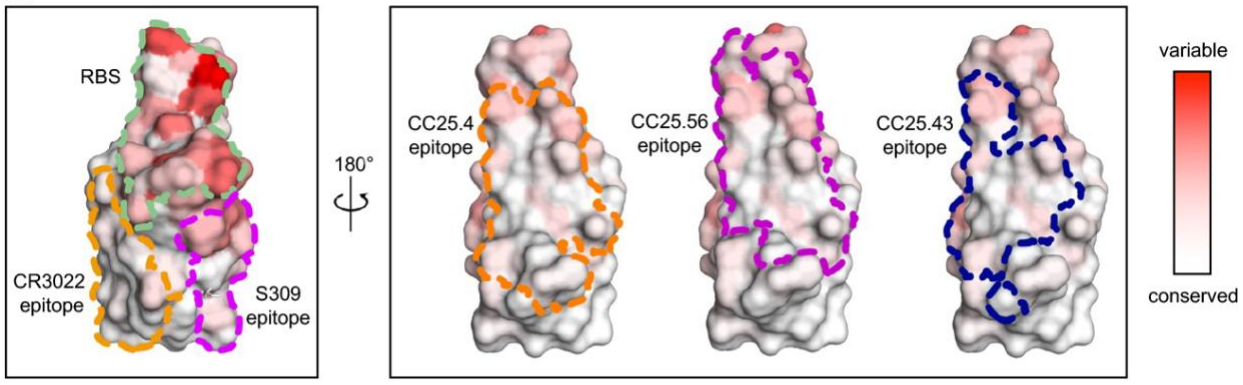

B

	344	345	346	347	348	351	352	353	354	355	356	357	359	360	393	394	396	399	426	428	429	430	457	458	459	461	462	463	464	465	466	467	468	469	470	471	472	473	474	481	482	492	514	515	516	517	518	519	520	521
WT	A	T	R	F	A	Y	A	W	N	R	K	R	S	N	T	N	Y	S	P	D	F	T	R	K	S	L	K	P	F	E	R	D	I	S	T	E	I	Y	Q	N	G	L	S	F	E	L	L	H	A	P
Alpha	-	-	-	-	-	-	-	-	-	-	-	-	-	-	-	-	-	-	-	-	-	-	-	-	-	-	-	-	-	-	-	-	-	-	-	-	-	-	-	-	-	-	-	-	-	-	-	-	-	-
Beta	-	-	-	-	-	-	-	-	-	-	-	-	-	-	-	-	-	-	-	-	-	-	-	-	-	-	-	-	-	-	-	-	-	-	-	-	-	-	-	-	-	-	-	-	-	-	-	-	-	-
Gamma	-	-	-	-	-	-	-	-	-	-	-	-	-	-	-	-	-	-	-	-	-	-	-	-	-	-	-	-	-	-	-	-	-	-	-	-	-	-	-	-	-	-	-	-	-	-	-	-	-	-
Delta	-	-	-	-	-	-	-	-	-	-	-	-	-	-	-	-	-	-	-	-	-	-	-	-	-	-	-	-	-	-	-	-	-	-	-	-	-	-	-	-	-	-	-	-	-	-	-	-	-	-
BA.1	-	-	-	-	-	-	-	-	-	-	-	-	-	-	-	-	-	-	-	-	-	-	-	-	-	-	-	-	-	-	-	-	-	-	-	-	-	-	-	-	-	-	-	-	-	-	-	-	-	-
BA.2	-	-	-	-	-	-	-	-	-	-	-	-	-	-	-	-	-	-	-	-	-	-	-	-	-	-	-	-	-	-	-	-	-	-	-	-	-	-	-	-	-	-	-	-	-	-	-	-	-	-
BA.4/5	-	-	-	-	-	-	-	-	-	-	-	-	-	-	-	-	-	-	-	-	-	-	-	-	-	-	-	-	-	-	-	-	-	-	-	-	-	-	-	-	-	-	-	-	-	-	-	-	-	-
BQ.1.1	-	-	T	-	-	-	-	-	-	-	-	-	-	-	-	-	-	-	-	-	-	-	-	-	-	-	-	-	-	-	-	-	-	-	-	-	-	-	-	-	-	-	-	-	-	-	-	-	-	-
XBB.1.5	-	-	T	-	-	-	-	-	-	-	-	-	-	-	-	-	-	-	-	-	-	-	-	-	-	-	-	-	-	-	-	-	-	-	-	-	-	-	-	-	-	-	-	-	-	-	-	-	-	-
CC25.4																																																			
CC25.56																																																			
CC25.43																																																			

C

	V heavy	V light	D gene
CC25.4	VH1-2	VL1-40	DH1-14
CC25.56	VH5-51	VL3-21	DH6-19
CC25.43	VH3-73	VK1-5	DH2-15
S2H97	VH5-51	VL2-14	No info*
COVOX-45	VH3-30-3	VK1-33	No info*
553-49	VH3-23	VL6-57	No info*
XMA09	VH1-69	VL3-21	No info*

Figure 6. CC25.4, and CC25.56, and CC25.43, target a highly conserved site on the spike RBD.

A. Locations of the receptor binding site (RBS, pale green) and antibody epitopes (orange, magenta, blue) are indicated by dashed lines [defined as RBD residues with BSA > 0 Å^2 as calculated by PISA]. A white-red spectrum is used to represent the conservation of each residue of sarbecoviruses including SARS-CoV-2 VOCs, SARS-CoV-1, etc. [70]

B. Sequence alignment of epitope residues of CC25.4, CC25.56, and CC25.43. Identical residues of each variant to the wild-type SARS-CoV-2 are represented by a dash '-'. Epitope residues for each antibody are represented as grey boxes.

C. Putative germline genes encoding site V antibodies as predicted by IgBLAST [56]. * No info: no D gene or nucleotide sequence information was found for the previously published antibodies S2H97, COVOX-45, 553-49, and XMA09.

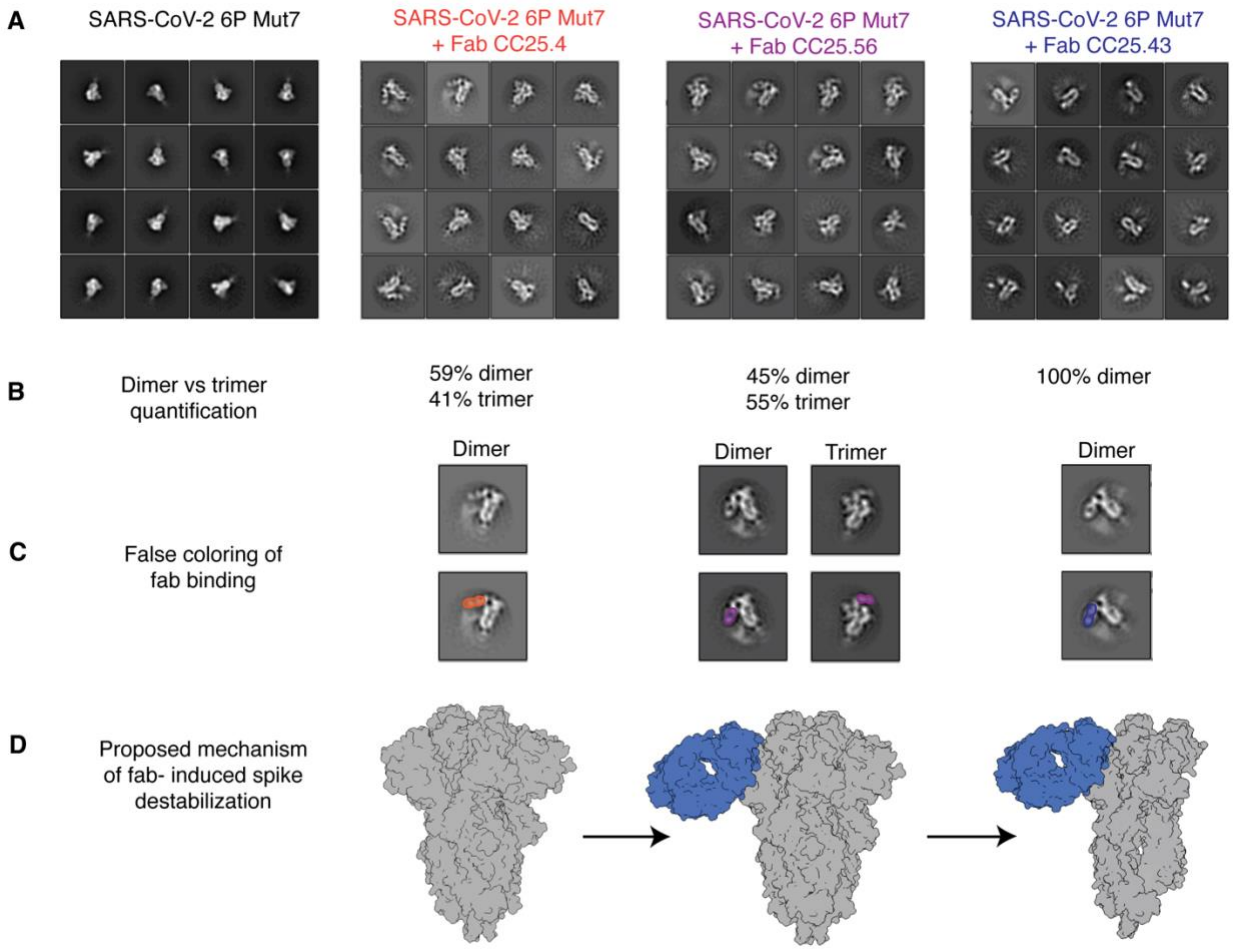

Figure 7. Group 2 RBD bnAbs destabilize the SARS-CoV-2 soluble spike.
A. Representative 2D classifications of SARS-CoV-2 6P Mut7 spike alone and SARS-CoV-2 6P Mut7 spike in complex with group 2 bnAbs, CC25.4, CC25.56, and CC25.43.
B. Dimer and trimer proportions were calculated from particle counts within each 2D class.
C. bnAb binding to the spike is highlighted using false coloring. BnAb binding to trimer was only observed with CC25.56. CC25.4 is colored orange, CC25.56 is colored purple, and CC25.43 is colored blue.
D. Proposed model of spike degradation induced by bnAb binding. Spike model taken from PDB (6VXX) [71]. BnAb positioning is approximated based on 2D classes and is colored blue.

MATERIAL AND METHODS

Expression and purification of spike and RBD proteins

Plasmids coding for the soluble S ectodomain proteins as well as the RBD of human coronaviruses were transfected into Freestyle293F cells (Thermo Fisher R79007). Per 1 L of Freestyle 293F cells, 350 µg of spike/RBD encoding plasmid was mixed with 40 ml transfectagro™ (Corning 40-300-CV) and filtered using 0.22 µm Steriflip™ Sterile Disposable Vacuum Filter Units (MilliporeSigma™ SCGP00525). After filtering, 1.6 mL of 40 K polyethylenimine (Polysciences 24765-1) (1 mg/mL) was added to the plasmid mixture. The resulting solution was gently mixed and then incubate at room temperature for 30 minutes before adding into a 1 L FreeStyle293F cell culture at a concentration of 1 x 10^6 cells ml^{-1}. Four days after transfection, the cell cultures were centrifuged at 2500 x g for 15 minutes and the resulting supernatants were filtered through 0.2 µm membrane filters (Fisher Scientific 564-0020). Cultures were then stored in glass bottles at 4°C before purification. Filtered supernatants containing His-tagged proteins were passed slowly through HisPur Ni-NTA Resin (Thermo Fisher 88221) beads in columns, washed with three bead volumes of wash buffer (25mM Imidazole, pH 7.4) to eliminate non-specific binding, and then slowly eluted with 25 ml of elution buffer (250mM Imidazole, pH 7.4). Eluted proteins were buffer exchanged into PBS and then concentrated down using Amicon® 100 kDa or 10 kDa Ultra-15 Centrifugal Filter Units (Merck Millipore UFC9100 & UFC9010), respectively, for spike and RBD proteins. The concentrated proteins were then further purified through size-exclusion chromatography using a Superdex 200 Increase 10/300 GL column (Sigma-Aldrich GE28-9909-44). Selected fractions resulting from the size-exclusion run were pooled together and concentrated again for later use.

Expression and purification of mAbs

For the expression of mAbs, HC and LC variable regions were cloned into expression vectors with corresponding constant regions. 12 µg plasmid of each chain were mixed into 3 ml Opti-MEM (Gibco 31985070), followed by adding 24 µl FectoPRO transfection reagent (116-040; Polyplus). After incubating at room temperature for 10 min, the mixture was gently added into Expi293F cells (Thermo Fisher Scientific A14527) at a concentration of 2.8 million cells ml^{-1} in final expression volumes of 30 ml. 24 h after transfection, 300 µl sodium valproic acid (300mM) and 275 µl 45% D-(+)-Glucose Solution, (Sigma G8769-100ML) were added. Five days after transfection, the cell cultures were centrifuged at 2500 x g for 15 minutes and the resulting supernatants were filtered using 0.22 µm Steriflip™ Sterile Disposable Vacuum Filter Units (MilliporeSigma™ SCGP00525). The filtered cell culture supernatants were incubated overnight at 4 °C with 0.5 ml 1:1 solution of Praesto Protein A Affinity Chromatography Resin (Purolite PR00300-164) and Protein G Sepharose (Cytiva GE17-0618-01). The solution was then loaded into an Econo-Pac column (Bio-Rad Laboratories 7321010) and washed with 1 column volume of PBS. The mAbs were then eluted with 10 ml 0.2M citric acid (pH 3) and immediately neutralized using 1 ml 2M Tris base (pH 9). The eluted proteins were buffer exchanged into PBS and then concentrated using Amicon® 30 kDa Ultra-15 Centrifugal Filter Units (Merck Millipore UFC9030).

Production of proteins for the BioLayer Interferometry (BLI) competition analysis

Expression and purification of the SARS-CoV-2 spike protein were done as described previously [28]. Briefly, the ectodomain (residues 14-1213) with R682G / R683G / R685G / K986P / V987P mutations of the SARS-CoV-2 spike protein (GenBank: QHD43416.1) was cloned into a customized pFastBac vector [72]. The spike ectodomain constructs were fused with an N-terminal gp67 signal peptide and a C-terminal BirA biotinylation site, thrombin cleavage site, trimerization domain, and His6 tag. Recombinant bacmid DNA was generated using the Bac-to-Bac system (Life Technologies). Baculovirus was generated by transfecting purified bacmid DNA into Sf9 cells using FuGENE HD (Promega), and subsequently used to infect suspension cultures of High Five cells (Life Technologies) at an MOI of 5 to 10. Infected High Five cells were incubated at 28 °C with shaking at 110 rpm for 72 h for protein expression. The supernatant was then concentrated using a Centramate cassette (30 kDa MW cutoff, Pall Corporation). SARS-CoV-2 Spike were purified by Ni-NTA, followed by size exclusion chromatography, and then buffer exchanged into PBS. Expression and purification of the N-terminal peptidase domain of human ACE2 (residues 19 to 615, GenBank: BAB40370.1) was described previously [73]. ACE2 was cloned into phCMV3 vector and fused with a C-terminal Fc tag. The plasmids were transiently transfected into Expi293F cells using ExpiFectamine™ 293 Reagent (Thermo Fisher Scientific) according to the manufacturer's instructions. The supernatant was collected at 7 days post-transfection. Fc-tagged ACE2 protein was then purified with a Protein A column (GE Healthcare) followed by size exclusion chromatography.

BioLayer Interferometry binding assay

Using an Octet RED384 instrument, BLI binding experiments were performed with Anti-Human IgG Fc (AHC) biosensors (Sartorius 18-5060). Using Octet buffer (PBS with 0.1% Tween20), mAbs were diluted to 10 μg ml^{-1}, while spike and RBD proteins were diluted to 100 nM and 275 nM, respectively. Samples were transferred to black Polypropylene 96-well F-Bottom Microplates (Greiner 655209) for BLI experimentation. The hydrated biosensors first captured the antibodies for 60 s, and then transferred to Octet buffer for 60 s to provide the baseline. The biosensors with captured antibodies were then introduced to the wells containing the viral proteins for 120 s to measure association responses, and into Octet buffer for 240 s to measure disassociation responses. Results from the experiment were analyzed with ForteBio Data Analysis software (version 12) for curve correction and fitting into a 1:1 binding mode. The binding response and KD values were calculated.

For the competition assays of antibodies with ACE2 receptor, Ni-NTA biosensors were used. In brief, the assay had five steps: 1) baseline: 60 s with 1× kinetics buffer; 2) loading: 360 s with 20 μg/mL, His6-tagged SARS-CoV-2 spike protein; 3) baseline: 60 s with 1× kinetics buffer; 4) first association: 360 s with Fabs (2 μM, or buffer only as a control); and 5) second association: 360 s with human ACE2-Fc (200 nM).

Pseudovirus production

The spike proteins of each tested virus were cloned into a plasmid expression vector with each protein's endoplasmic reticulum retrieval signal removed. These plasmids were co-transfected with MLV (murine leukemia virus)-CMV (cytomegalovirus) luciferase and MLV

Gag/Pol plasmids into HEK-293T cells (ATCC CRL-3216) using Lipofectamine 2000 (Thermo Fisher 11668019) transfection reagent following the manufacturer's recommended protocol. 16 hours after transfection, cell media was replaced with fresh warm cell media (DMEM (Corning 10-017-CV) with 10% FBS (Omega Scientific NC0471611), 1% L-glutamine (Corning 25-005-CI), and 1% penicillin-streptomycin (Corning 30-002-CI)). 48 hours after transfection, supernatant was collected and filtered using 0.22 µm Steriflip™ Sterile Disposable Vacuum Filter Units (MilliporeSigma™ SCGP00525) and the resulting pseudoviruses were stored at −80 °C for later use.

Pseudovirus neutralization assay

We first developed hACE2 expressing cells by transducing hACE2 into HeLa cells (ATCC CCL-2) using a lentivirus system. Cells with stable and high hACE2 expression were selected to be used for the pseudovirus neutralization assay. For the neutralization assay, mAbs were diluted to a starting concentration of 60 µg ml^{-1} in cell media (DMEM (Corning 10-017-CV) with 10% FBS (Omega Scientific NC0471611), 1% L-glutamine (Corning 25-005-CI), and 1% penicillin-streptomycin (Corning 30-002-CI)) and then three-folds serially diluted. 25 µl of each dilution was added to 96 half-area well plates (Corning 3688) and incubated with 25 µl pseudoviruses per well at 37°C for 1 hour. HeLa-hACE2 cells were diluted in cell media to 2 x 10^5 cells ml^{-1}. 50 µl of diluted cells containing 20 µg ml^{-1} DEAE-dextran (Sigma-Aldrich 93556-1G) were added to each well. After 48 hours of incubation at 37°C, supernatant was removed and HeLa-hACE2 cells were lysed with 60 µl per well of a solution containing luciferase lysis buffer (25 mM Gly-Gly, pH 7.8, 15 mM MgSO4, 4 mM EGTA, 1% Triton X-100) and Bright-Glo (Promega Corporation E2620) at a 1:10 ratio. Wells of lysed cells containing Bright Glo were analyzed for luciferase activity using a luminometer. Each mAb was tested in duplicate and repeated independently. Percent neutralization was determined using the equation below:

Percentage neutralization = 100 × (1 − ((RLU of sample)−(Average RLU of CC))/((Average RLU of VC)−(Average RLU of CC)))

Neutralization percentage was calculated and plotted in Prism 8 (Graph Pad Software) and the IC_{50} antibody titers were determined by fitting a non-linear regression curve and determining the antibody concentration at 50% pseudovirus neutralization.

Production of proteins for structure analysis

Expression and purification of the SARS-CoV-2 spike receptor-binding domain (RBD) for crystallization were as described previously [28]. Briefly, the wild-type RBD (residues 333-529) of the spike (S) proteins was cloned into a customized pFastBac vector [74], and fused with an N-terminal gp67 signal peptide and C-terminal His_6 tag [28]. The recombinant bacmid DNA was generated using the Bac-to-Bac system (Life Technologies). Baculoviruses were generated by transfecting purified bacmid DNAs into Sf9 cells using FuGENE HD (Promega), and subsequently used to infect suspension cultures of High Five cells (Life Technologies) at an MOI of 5 to 10. Infected High Five cells were incubated at 28 °C with shaking at 110 r.p.m. for 72 h for protein expression. The supernatants were then concentrated using a 10 kDa MW cutoff Centramate cassette (Pall Corporation). The RBD protein was purified by Ni-NTA, followed by size exclusion chromatography, and buffer exchanged into 20 mM Tris-HCl pH 7.4 and 150 mM NaCl.

Fabs used for crystallization were expressed and purified as follows: the plasmids of heavy and light chains were transiently co-transfected into Expi293F cells using FectoPRO transfection reagent (116-040; Polyplus) according to the manufacturer's instructions. The supernatant was collected at 5 days post-transfection. The Fab was purified with a CaptureSelect CH1-XL Pre-packed Column (Thermo Fisher Scientific) followed by size exclusion chromatography. VSRRLP and VFNQIKP variants of the elbow region was used to reduce the conformational flexibility between the heavy chain constant and variable domains of Fabs CC25.4 and CC25.56, respectively, for crystallization [75]. For CC25.43, both the heavy and light chains were mutated to facilitate crystal packing. A VFNQIKG mutation was applied to the elbow region of the heavy chain [75], and the FG loop of the kappa chain (HQGLSSP) was shortened to QGTTS to facilitate edge-to-edge beta-sheet packing [76]. Other structures in this paper were obtained from crystallization with unmutated Fabs and RBD.

Fabs used for ns-EM were purified as follows: expressed IgGs were concentrated and digested using the Pierce™ Fab Preparation Kit (Thermo Fisher 44985) following manufacturer instructions. The resulting Fabs were buffer exchanged into PBS and then concentrated down using Amicon® 10 kDa Ultra-15 Centrifugal Filter Units (Merck Millipore UFC9010). Selected fractions resulting from the size-exclusion chromatography were pooled together and concentrated again for later use.

Crystallization and structural determination

CC25.4/RBD, CC25.36/RBD/CV38-142, CC25.54/RBD, CC25.43/RBD, CC25.56/RBD, CC84.2/RBD, CC84.24/RBD complexes were formed by mixing each of the protein components in an equimolar ratio and incubating overnight at 4°C. The protein complexes were adjusted to 8.6–12 mg/ml and screened for crystallization using the 384 conditions of the JCSG Core Suite (Qiagen) on our robotic CrystalMation system (Rigaku) at Scripps Research. Crystallization trials were set-up by the vapor diffusion method in sitting drops containing 0.1 µl of protein and 0.1 µl of reservoir solution. For the CC25.4/RBD complex, optimized crystals were grown in drops containing 65% MPD and 0.1 M Bicine pH 9.0 at 20°C. Crystals appeared on day 28 and were harvested on day 30. Diffraction data were collected at cryogenic temperature (100 K) at beamline 23-ID-B of the Advanced Photon Source (APS) at Argonne National Labs. For the CC25.36/RBD/CV38-142 complex, optimized crystals were grown in drops containing 20% (w/v) PEG-3350 and 0.2 M di-ammonium citrate at 20°C. Crystals appeared on day 7 and were harvested on day 15. Diffraction data were collected at cryogenic temperature (100 K) at beamline 12-1 of the Stanford Synchrotron Radiation Lightsource (SSRL). For the CC25.54/RBD complex, optimized crystals were grown in drops containing 20% (w/v) PEG-3350 and 0.2 M potassium sodium tartrate pH 7.2 at 20°C. Crystals appeared on day 28 and were harvested on day 45. Diffraction data were collected at cryogenic temperature (100 K) at beamline 23-ID-B of the Advanced Photon Source (APS) at Argonne National Labs. For the CC25.43/RBD complex, optimized crystals were grown in drops containing 1.0 M Li-chloride, 10% PEG-6000, and 0.1 M citric acid pH 4.0 at 20°C. Crystals appeared on day 7 and were harvested on day 15 by soaking in reservoir solution supplemented with 20% (v/v) ethylene glycol. Diffraction data were collected at cryogenic temperature (100 K) at beamline 23-ID-B of the APS. The B-values of the RBD molecules in the CC25.43/RBD complex structure are higher than the overall average B-values because a large region

of the RBDs is exposed in the crystal with lack of stabilization from crystal packing. For the CC25.56/RBD complex, optimized crystals were grown in drops containing 10% ethylene glycol (v/v), 0.11 M $MgCl_2$, and 16% polyethylene glycol 3350 (w/v) at 20°C. Crystals appeared on day 7 and were harvested on day 15 with no additional cryoprotectant. Diffraction data were collected at cryogenic temperature (100 K) at beamline 23-ID-D of the APS. For the CC84.2/RBD complex, optimized crystals were grown in drops containing 20% (w/v) PEG-3000 and 0.1 M sodium citrate pH 5.5 at 20°C. Crystals appeared on day 21 and were harvested on day 45. Diffraction data were collected at cryogenic temperature (100 K) at beamline 23-ID-B of the APS. For the CC84.24/RBD complex, optimized crystals were grown in drops containing 20% (w/v) PEG-3000 and 0.1 M Sodium citrate pH 5.5 at 20°C. Crystals appeared on day 21 and were harvested on day 45. Diffraction data were collected at cryogenic temperature (100 K) at beamline 23-ID-B of the APS. Diffraction data were processed with either HKL2000 (PubMed: 27754618) or AutoPROC [77]. Structures were solved by molecular replacement using PHASER [78]. Iterative model building and refinement were carried out in COOT [79] and PHENIX [80], respectively. Epitope and paratope residues, as well as their interactions, were identified by accessing PISA at the European Bioinformatics Institute (http://www.ebi.ac.uk/pdbe/prot_int/pistart.html) [81].

Negative stain electron microscopy

SARS-CoV-2 6P Mut7 and monoclonal bnAbs were complexed at a 3:1 molar ratio (Fab:spike) for one hour at room temperature and SEC purified using a Superose 6 Increase 10/300 GL column in an AKTA Pure system. nsEM grids were made by depositing 3 µl of complex at a dilution of ~0.03 mg/ml and stained with 2% uranyl formate for 90 seconds. Grids were imaged using a Thermo Fisher Falcon 4i Direct Electron Detector 4K x 4K camera on a Thermo Fisher Glacios (200 kEV, 73kx mag) and micrographs were processed in Relion 3.1 [82]. Particles from raw micrographs were picked using a Laplacian-of-Gaussian spatial filter and classified into 2D classes. Cartoon figures were made in ChimeraX [83].

Statistical analysis

Statistical analysis was performed using Graph Pad Prism 8, Graph Pad Software, San Diego, California, USA. IC_{50} neutralization titers or BLI binding responses were compared using the non-parametric unpaired Mann-Whitney-U test. Data were considered statistically significant when $p < 0.05$.

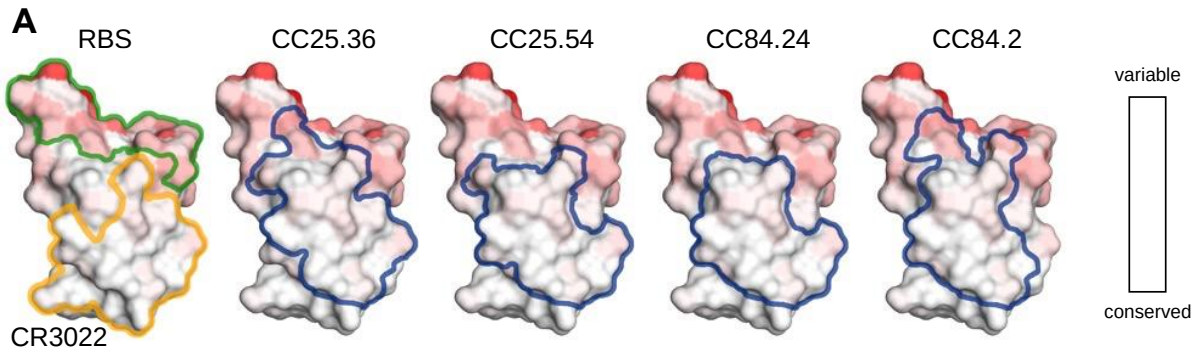

B

	368	369	370	371	372	374	375	376	377	378	379	380	381	382	383	384	385	403	404	405	406	407	408	409	411	412	413	414	415	416	417	420	421	424	427	428	429	430	455	456	460	504	505
WT	**L**	**Y**	**N**	**S**	**A**	**F**	**S**	**T**	**F**	**K**	**C**	**Y**	**G**	**V**	**S**	**P**	**T**	**R**	**G**	**D**	**E**	**V**	**R**	**Q**	**A**	**P**	**G**	**Q**	**T**	**G**	**K**	**D**	**D**	**K**	**D**	**D**	**F**	**T**	**L**	**F**	**N**	**G**	**Y**
Alpha	-	-	-	-	-	-	-	-	-	-	-	-	-	-	-	-	-	-	-	-	-	-	-	-	-	-	-	-	-	-	-	-	-	-	-	-	-	-	-	-	-	-	-
Beta	-	-	-	-	-	-	-	-	-	-	-	-	-	-	-	-	-	-	-	-	-	-	-	-	-	-	-	-	-	-	N	-	-	-	-	-	-	-	-	-	-	-	-
Gamma	-	-	-	-	-	-	-	-	-	-	-	-	-	-	-	-	-	-	-	-	-	-	-	-	-	-	-	-	-	-	T	-	-	-	-	-	-	-	-	-	-	-	-
Delta	-	-	-	-	-	-	-	-	-	-	-	-	-	-	-	-	-	-	-	-	-	-	-	-	-	-	-	-	-	-	-	-	-	-	-	-	-	-	-	-	-	-	-
BA.1	-	-	-	L	-	-	F	-	-	-	-	-	-	-	-	-	-	-	-	-	-	-	-	-	-	-	-	-	-	-	N	-	-	-	-	-	-	-	-	-	-	-	H
BA.2	-	-	-	F	-	-	F	A	-	-	-	-	-	-	-	-	-	-	-	N	-	-	S	-	-	-	-	-	-	-	N	-	-	-	-	-	-	-	-	-	-	-	H
BA.4/5	-	-	-	F	-	-	F	A	-	-	-	-	-	-	-	-	-	-	-	N	-	-	S	-	-	-	-	-	-	-	N	-	-	-	-	-	-	-	-	-	K	-	H
BQ.1.1	-	-	-	F	-	-	F	A	-	-	-	-	-	-	-	-	-	-	-	N	-	-	S	-	-	-	-	-	-	-	N	-	-	-	-	-	-	-	-	-	K	-	H
XBB.1.5	I	-	-	F	-	-	F	A	-	-	-	-	-	-	-	-	-	-	-	N	-	-	S	-	-	-	-	-	-	-	N	-	-	-	-	-	-	-	-	-	K	-	H
CC25.36																																											
CC25.54																																											
CC84.2																																											
CC84.24																																											

Figure S1. Group 1 RBD bnAb target a relatively conserved site targeted by class 4 bnAbs.

A. Locations of the receptor binding site (RBS, pale green) and RBD class 4 site CR3022 antibody epitope (orange) are indicated by outlines [defined as RBD residues with buried surface area (BSA) > 0 Å^2 as calculated by PISA]. A white-red spectrum is used to represent the conservation of each residue of sarbecoviruses including SARS-CoV-2 VOCs, SARS-CoV-1, etc. as in the Figure 6A.

B. Sequence alignment of epitope residues of group 1 RBD bnAbs, CC25.36, CC25.54, CC84.2 and CC84.24. Identical residues of each variant to the wild-type SARS-CoV-2 are represented by a dash '-'. Epitope residues for each antibody are represented as grey boxes.

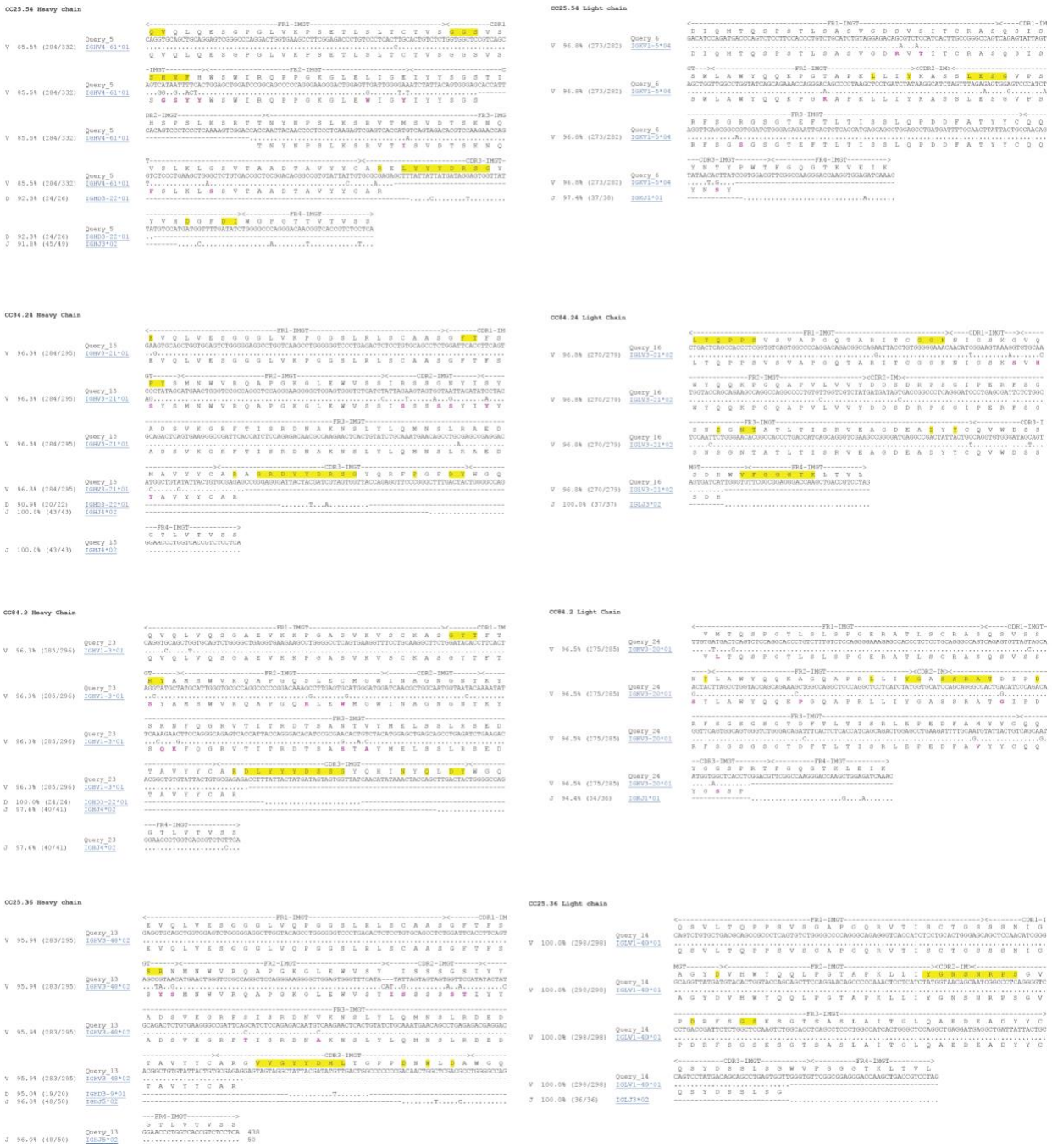

Figure S2. Alignment of group 1 RBD broadly neutralizing antibodies and their putative germline sequences.

Paratope residues [defined as buried surface area (BSA) > 0 Å^2 as calculated by PISA [81] of group 1 RBD bnAbs, CC25.54, CC84.24, CC84.2 and CC25.36 are highlighted with yellow boxes. Germline residues that have been somatically mutated as calculated by IgBLAST [56] are highlighted in purple.

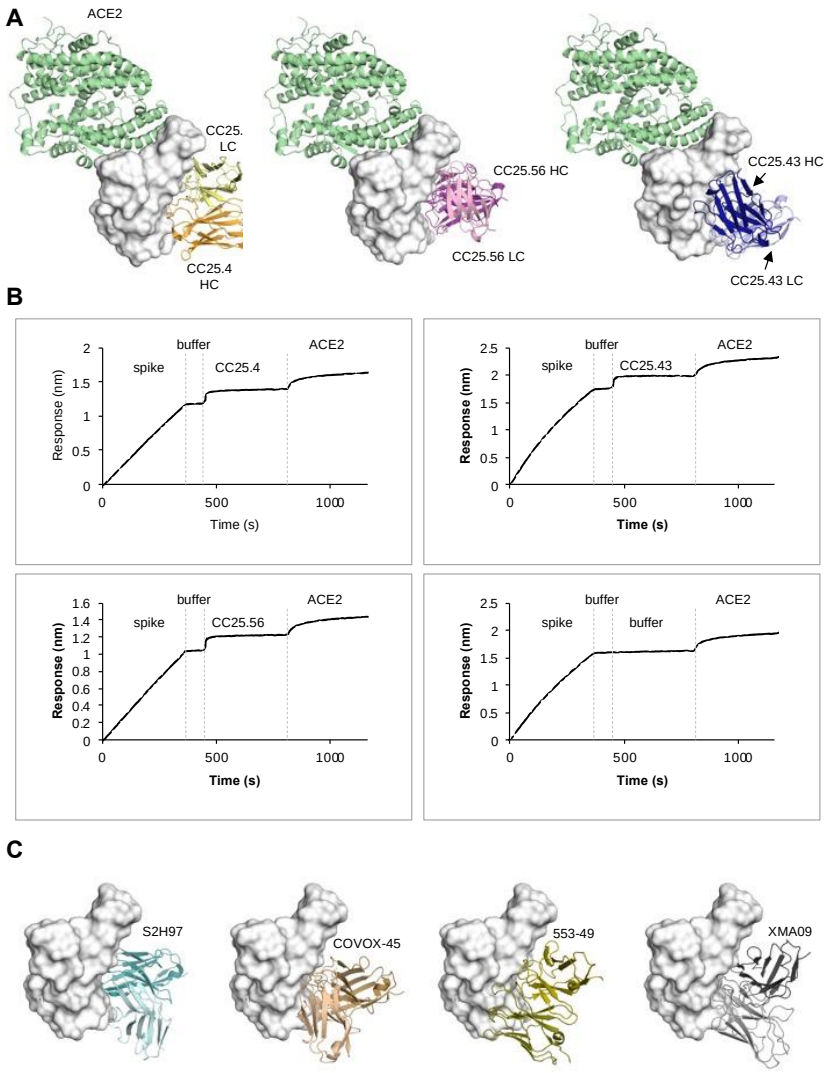

Figure S3. Structures of antibodies targeting site V of SARS-CoV-2 RBD. The SARS-CoV-2 RBD is shown in white.

A. The structure of SARS-CoV-2 RBD in complex with human receptor ACE2 (PDB 6M0J) was superimposed onto the structures of RBD in complex with site-V antibodies determined in this study. ACE2 is in pale green. Heavy and light chains of CC25.4 are in orange and yellow, while those of CC25.56 in dark and light pink, and CC25.43 in dark and light blue, respectively.

B. Biolayer interferometry assay of ACE2 binding to SARS-CoV-2 S protein in the presence of site V targeting Fabs.

C. Comparison with previously reported site-V antibodies. Antibodies S2H97 (PDB 7M7W), COVOX-45 (PDB 7ORA), 553-49 (PDB 7WOG), and XMA09 (PDB 7WHZ) are shown in teal, sand, olive, and grey, respectively (heavy and light chains in dark and light colors).

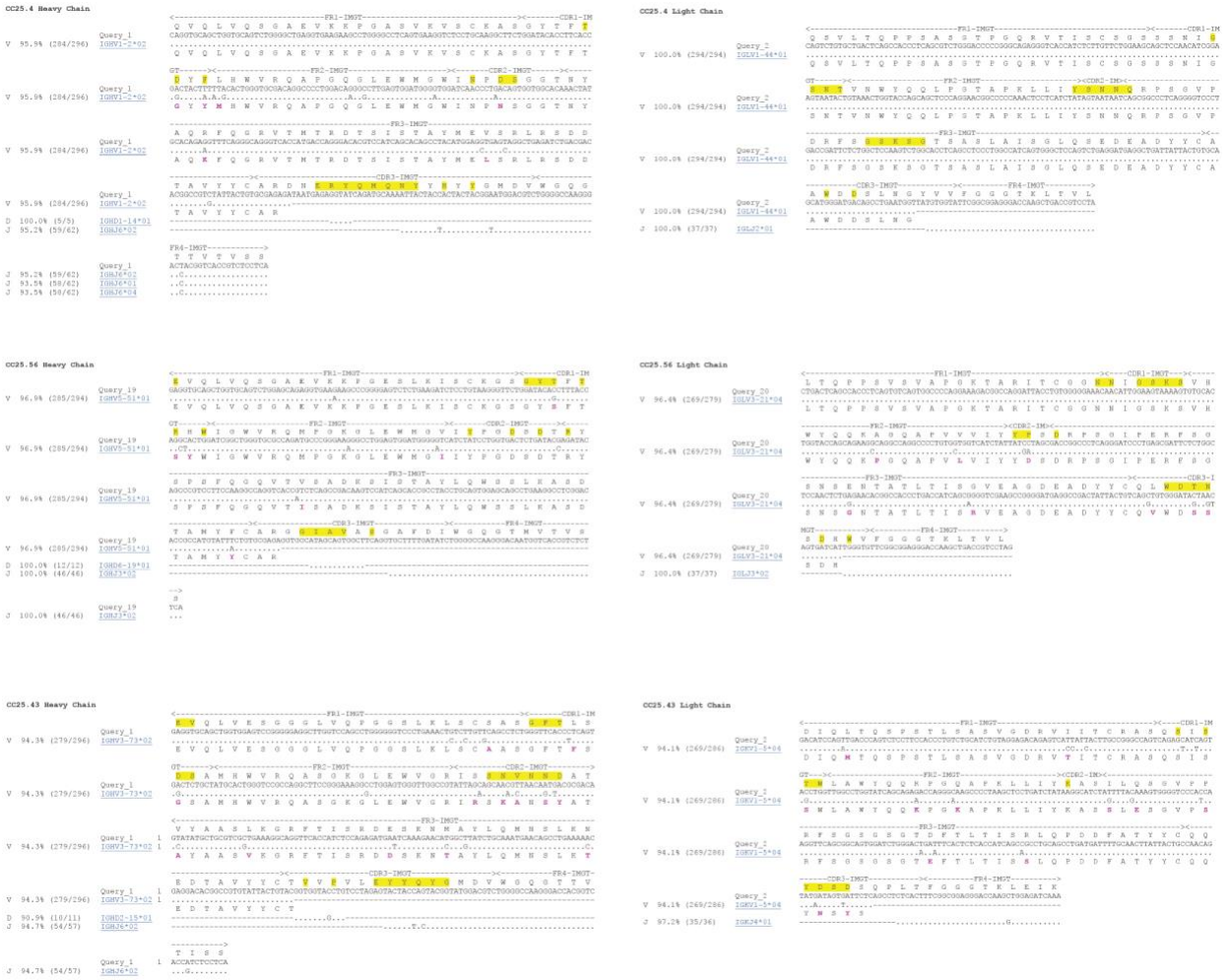

Figure S4. Alignment of group 1 and group 2 RBD broadly neutralizing antibodies and their putative germline sequences.

Paratope residues [defined as buried surface area (BSA) > 0 Å^2 as calculated by PISA [81] of group 2 RBD bnAbs, CC25.4, CC25.56 and CC25.43 are highlighted with yellow boxes. Germline residues that have been somatically mutated as calculated by IgBLAST [56] are highlighted in purple.

		Mature bnAbs													bnAb inferred germline (iGL) versions													Other Sarbecoviruses					
		SARS-CoV-2													SARS-CoV-2													Pang17		SARS-1		WIV1	
Group (RBD)	mAb ID	WT	Alpha	Beta	Gamma	Delta	BA.1	BA.2	BA.2.12.1	BA.2.75	BA.4/5	BQ.1.1	XBB	XBB.1.5	WT	Alpha	Beta	Gamma	Delta	BA.1	BA.2	BA.2.12.1	BA.2.75	BA.4/5	BQ.1.1	XBB	XBB.1.5	Mature	iGL	Mature	iGL	Mature	iGL
1	CC25.1	0.11	0.04	0.09	0.07	0.07	0.79	15.0	7.42	23.1	9.31	13.5	>30	>30	0.14	0.03	0.05	0.05	0.06	>30	>30	>30	>30	>30	>30	>30	>30	0.12	>30	0.03	1.46	0.01	0.04
1	CC25.3	0.20	0.17	0.21	0.19	0.17	0.75	7.80	2.55	10.3	4.91	5.26	2.18	6.34	3.39	>30	0.23	0.34	0.25	>30	>30	>30	>30	>30	>30	>30	>30	0.09	3.03	0.20	>30	0.02	1.65
1	CC25.13	0.21	0.16	0.18	0.18	0.16	>30	>30	>30	>30	>30	>30	>30	>30	>30	>30	17.5	1.58	0.25	>30	>30	>30	>30	>30	>30	>30	>30	>30	>30	2.93	>30	0.01	3.68
1	CC25.36	0.18	0.13	0.14	0.16	0.21	0.30	12.7	3.84	12.8	4.57	11.1	4.39	10.7	1.04	2.44	0.41	0.61	1.16	>30	>30	>30	>30	>30	>30	>30	>30	0.09	2.10	0.05	>30	0.03	0.88
1	CC25.48	0.56	0.41	0.27	0.36	0.38	>30	>30	>30	>30	>30	>30	>30	>30	>30	>30	9.21	3.29	0.51	>30	>30	>30	>30	>30	>30	>30	>30	0.13	>30	0.34	>30	0.08	19.5
1	CC25.52	0.17	0.10	0.20	0.14	0.12	1.63	>30	>30	>30	>30	>30	>30	>30	>30	>30	24.8	27.4	18.2	>30	>30	>30	>30	>30	>30	>30	>30	0.09	>30	0.04	>30	0.01	>30
1	CC25.53	0.25	0.17	0.40	0.50	0.33	9.35	>30	>30	>30	>30	>30	>30	>30	0.63	0.09	0.24	0.17	0.23	7.62	>30	>30	>30	>30	>30	>30	>30	0.10	0.42	0.10	0.31	0.01	0.15
1	CC25.54	0.24	0.18	0.21	0.17	0.20	0.52	21.2	4.17	25.1	16.6	>30	7.46	8.40	>30	>30	1.47	3.27	0.95	>30	>30	>30	>30	>30	>30	>30	>30	0.06	>30	0.04	>30	0.02	>30
1	CC84.2	0.63	0.76	0.41	0.63	1.14	>30	>30	>30	>30	>30	>30	>30	>30	0.97	0.73	0.71	0.25	0.33	9.63	>30	>30	>30	>30	>30	>30	>30	0.08	0.29	4.45	>30	0.08	0.39
1	CC84.5	0.12	0.08	0.16	0.11	0.13	>30	>30	>30	>30	>30	>30	>30	>30	3.39	0.72	0.17	0.15	0.16	>30	>30	>30	>30	>30	>30	>30	>30	0.08	>30	0.06	>30	0.07	>30
1	CC84.10	0.21	0.13	0.20	0.16	0.24	0.68	>30	>30	>30	>30	>30	>30	>30	10.9	>30	0.88	0.70	1.51	>30	>30	>30	>30	>30	>30	>30	>30	0.08	>30	0.03	>30	0.01	>30
1	CC84.12	0.38	0.32	0.50	0.31	0.39	18.3	>30	>30	>30	>30	>30	>30	>30	>30	>30	>30	>30	>30	>30	>30	>30	>30	>30	>30	>30	>30	0.26	>30	0.19	>30	0.06	>30
1	CC84.21	0.26	0.23	0.24	0.23	0.38	1.14	>30	>30	>30	>30	>30	>30	>30	>30	>30	>30	>30	>30	>30	>30	>30	>30	>30	>30	>30	>30	0.20	>30	0.56	>30	0.06	>30
1	CC84.24	0.12	0.30	0.26	0.27	0.22	0.79	28.1	5.88	10.6	2.43	7.27	4.38	5.57	>30	>30	1.22	>30	>30	>30	>30	>30	>30	>30	>30	>30	>30	0.10	>30	0.15	>30	0.01	>30
2	CC25.4	0.53	0.31	0.74	0.35	0.76	0.98	2.38	1.50	3.53	1.64	9.72	7.62	2.20	>30	>30	>30	>30	>30	>30	>30	>30	>30	>30	>30	>30	>30	0.46	>30	0.21	>30	0.02	>30
2	CC25.17	2.18	1.08	1.13	1.40	2.18	2.54	10.7	4.28	7.07	6.25	>30	15.4	5.16	>30	>30	>30	>30	>30	>30	2.01	>30	>30	>30	>30	>30	>30	0.54	>30	0.16	>30	0.75	>30
2	CC25.42	3.19	2.15	2.21	2.46	3.93	8.95	8.97	>30	16.2	>30	>30	>30	>30	>30	>30	>30	>30	>30	>30	>30	>30	>30	>30	>30	>30	>30	7.07	>30	0.22	>30	1.42	>30
2	CC25.43	1.26	0.56	0.61	0.55	0.71	1.02	1.41	0.66	0.96	0.95	>30	12.8	6.9	>30	>30	>30	>30	>30	>30	>30	>30	>30	>30	>30	>30	>30	0.03	>30	0.22	>30	0.02	6.70
2	CC25.56	1.04	0.50	1.30	0.82	1.29	1.91	2.03	1.04	1.54	1.30	5.13	5.11	2.87	>30	>30	>30	>30	>30	>30	>30	>30	>30	>30	>30	>30	>30	0.20	>30	0.63	>30	0.03	>30
Control mAbs	S2X259	0.04	0.08	0.05	0.01	0.02	0.47	>30	>30	>30	>30	>30	>30	>30	>30	>30	>30	>30	>30	>30	>30	>30	>30	>30	>30	>30	>30	0.22	>30	0.04	>30	0.02	>30
	C022	0.10	0.13	0.25	0.03	0.04	>30	>30	>30	>30	>30	>30	>30	>30	21.5	>30	7.76	0.48	0.50	>30	>30	>30	>30	>30	>30	>30	>30	0.30	6.52	0.88	>30	0.10	29.2
	ADI56046	0.16	0.11	0.16	0.12	0.05	>30	>30	>30	>30	>30	>30	>30	>30	>30	>30	>30	>30	>30	>30	>30	>30	>30	>30	>30	>30	>30	>30	>30	0.04	>30	0.03	>30
	DH1047	0.17	0.07	0.06	0.05	0.02	>30	>30	>30	>30	>30	>30	>30	>30	>30	>30	>30	>30	>30	>30	>30	>30	>30	>30	>30	>30	>30	0.11	>30	0.13	>30	0.03	>30
	S309	>30	>30	6.11	>30	>30	4.25	9.09	12.2	5.12	16.9	4.28	1.20	3.08	>30	>30	>30	>30	>30	>30	>30	>30	>30	>30	>30	>30	>30	0.55	>30	0.12	>30	0.10	>30
	CC12.1	0.03	0.24	>30	6.82	0.05	>30	>30	>30	>30	>30	>30	>30	>30	ND	ND	ND	ND	ND	ND	ND	ND	ND	ND	ND	ND	ND	>30	ND	>30	ND	>30	ND
	DEN3	>30	>30	>30	>30	>30	>30	>30	>30	>30	>30	>30	>30	>30	ND	ND	ND	ND	ND	ND	ND	ND	ND	ND	ND	ND	ND	>30	ND	>30	ND	>30	ND

IC_{50} Neutralization (μg/ml) 0.01 | 0.1 | 1 | 10 | 30 | >30

Table S1. IC_{50} Neutralization of group 1 and 2 bnAbs and their inferred germline antibodies.

Experimentally determined neutralization IC_{50}s of the mature and inferred germline (iGL) versions of 14 Group 1 and 5 Group 2 RBD bnAbs tested with pseudotyped versions of SARS-CoV-2 (Wuhan), 12 SARS-CoV-2 Variants of Concern (B.1.1.7 (Alpha), B.1.351 (Beta), P.1 (Gamma), Delta (B.1.617.2), BA.1 (Omicron), BA.2, BA.2.12.1, BA.2.75, BA.4/5, BQ.1.1, XBB, XBB.1.5), and 3 other sarbecoviruses (Pang17 (Clade 1b), SARS-CoV-1 (Clade 1a), and WIV1 (Clade 1a)). Control Abs used were SARS-CoV-2 antibodies S2X259, C022, ADI56046, DH1047, S309, and CC12.1, and the Dengue antibody, DEN3. All experiments were conducted independently twice and verified to produce similar results. ND = Not Determined.

		Spike					RBD				
	Clade	SARS-2 (Clade 1b)		Clade 1a	Clade 2	Clade 3	SARS-2 (Clade 1b)		Clade 1a	Clade 2	Clade 3
Group (RBD)	mAb ID	WT	BA.4/5	SARS-1	RmYN02	BM-4831	WT	BA.4/5	SARS-1	RmYN02	BM-4831
1	CC25.1	1.03	1.18	1.00	0.75	1.17	0.45	0.24	0.55	0.02	0.43
1	CC25.3	0.92	0.93	0.80	0.87	0.87	0.46	0.61	0.54	0.17	0.23
1	CC25.13	0.96	0.27	0.66	0.26	0.40	0.48	0.05	0.47	0.00	0.01
1	CC25.36	0.92	0.86	0.70	0.72	0.75	0.43	0.53	0.51	0.45	0.43
1	CC25.48	0.66	0.03	0.53	0.67	0.76	0.45	0.05	0.47	0.37	0.37
1	CC25.52	1.02	0.87	0.83	0.44	0.96	0.50	0.08	0.51	0.00	0.26
1	CC25.53	0.90	0.83	0.77	0.93	1.04	0.43	0.55	0.45	0.44	0.29
1	CC25.54	1.02	0.54	0.80	0.92	1.05	0.49	0.46	0.49	0.50	0.47
1	CC84.2	0.78	0.38	0.47	0.78	0.84	0.43	0.34	0.44	0.15	0.33
1	CC84.5	0.95	0.04	0.74	0.02	0.89	0.46	0.05	0.47	0.01	0.37
1	CC84.10	0.92	0.87	0.51	0.85	0.96	0.41	0.25	0.53	0.07	0.39
1	CC84.12	0.91	0.23	0.50	0.76	0.07	0.43	0.05	0.50	0.10	0.00
1	CC84.21	0.89	0.49	0.52	0.57	1.08	0.43	0.05	0.46	0.39	0.25
1	CC84.24	0.95	0.95	0.78	1.09	0.67	0.43	0.62	0.52	0.20	0.02
2	CC25.4	0.95	1.04	0.90	1.25	1.37	0.48	0.82	0.51	0.46	0.25
2	CC25.17	0.94	1.00	0.60	0.99	1.18	0.47	0.69	0.51	0.42	0.48
2	CC25.42	0.83	0.94	0.48	0.80	0.85	0.52	0.67	0.54	0.45	0.45
2	CC25.43	0.79	0.96	0.53	0.96	0.33	0.42	0.60	0.49	0.10	0.01
2	CC25.56	0.89	0.87	0.70	0.93	1.26	0.42	0.61	0.46	0.41	0.27
Control mAbs	S2X259	1.00	0.71	0.76	0.40	0.88	0.47	0.27	0.49	0.10	0.41
	C022	0.83	0.57	0.45	0.88	0.48	0.47	0.35	0.49	0.20	0.06
	ADI56046	1.13	0.04	0.79	0.02	0.71	0.41	0.07	0.48	0.07	0.23
	DH1047	0.82	0.31	0.59	0.52	0.53	0.47	0.04	0.52	0.40	0.41
	S309	0.75	0.57	0.66	0.01	0.33	0.29	0.34	0.52	0.00	0.06
	CC12.1	0.58	0.02	0.00	0.02	0.02	0.30	0.05	0.00	0.00	0.00
	DEN3	0.00	0.03	0.00	0.02	0.04	0.00	0.05	0.00	0.00	0.00

BLI response (nm)	
1	
0.5	
0.1	
<0.1	

Table S2. BLI binding responses.

BLI response values (nm) of 14 Group 1 and 5 Group 2 RBD bnAbs binding to the trimeric spike proteins and monomeric RBD proteins of Clade 1b (SARS-CoV-2 and BA.4/5), Clade 1a (SARS-CoV-1), Clade 2 (RmYN02), and Clade 3 (BM-4831) betacoronaviruses. Control antibodies used were SARS-CoV-2 Abs S2X259, C022, ADI56046, DH1047, S309, and CC12.1, and the Dengue antibody DEN3.

Table S3. X-ray data collection and refinement statistics

Data collection	CC25.36 Fab + SARS-CoV-2 RBD + CV38-142 Fab	CC25.54 Fab + SARS-CoV-2 RBD	CC84.2 Fab + SARS-CoV-2 RBD	CC84.24 Fab + SARS-CoV-2 RBD
Beamline	SSRL 12-1	APS 23-IDB	APS 23-IDB	APS 23-IDB
Wavelength (Å)	0.97946	0.97930	1.03317	1.03317
Space group	*P* 2_1 2_1 2_1	*P* 3_2 2 1	*P* 1 2_1 1	*P* 2_1 2_1 2_1
Unit cell parameters				
a, b, c (Å)	60.4, 77.0, 266.4	135.9, 135.9, 87.1	68.7, 80.2, 73.5	101.4, 106.0, 247.0
α, β, γ (°)	90, 90, 90	90, 90, 90	90, 94.9, 90	90, 90, 90
Resolution (Å) [a]	50.0–2.50 (2.54–2.50)	50.0-3.30 (3.36-3.30)	50.0-3.08 (3.15-3.08)	50.0 –2.91 (2.95–2.91)
Unique reflections [a]	38,811 (1,970)	14,256 (705)	14,522 (706)	54,891 (2,362)
Redundancy [a]	3.5 (3.3)	11.5 (7.1)	4.2 (4.2)	6.2 (3.5)
Completeness (%) [a]	87.8 (92.0)	99.8 (98.7)	97.9 (97.0)	92.5 (81.3)
$\langle I/\sigma_I \rangle$ [a]	7.9 (1.1)	8.0 (2.0)	6.3 (1.0)	6.9 (1.2)
R_{sym}[b] (%) [a]	15.7 (>100)	29.8 (97.8)	20.5 (>100)	21.4 (76.6)
R_{pim}[b] (%) [a]	8.8 (66.0)	9.1 (38.1)	11.2 (63.6)	8.9 (43.0)
$CC_{1/2}$[c] (%) [a]	98.0 (51.5)	98.8 (32.1)	99.2 (71.7)	98.3 (42.1)
Refinement statistics				
Resolution (Å)	38.5-2.50	48.8–3.30	48.0-3.08	48.7-2.91
Reflections (work)	32,649	10,644	10,876	44,227
Reflections (test)	1,635	542	563	2,275
R_{cryst}[d] / R_{free}[e] (%)	24.7/28.7	20.8/23.6	25.6/30.3	26.1/30.9
No. of atoms	7,963	4,803	4,647	18,011
Macromolecules	7,914	4,789	4,633	17,983
Glycans	49	14	14	28
Average *B*-value (Å^2)	50	68	78	66
Macromolecules	50	68	78	66
Fab	51	67	70	70
RBD	46	70	96	58
Glycans	48	87	127	67
Wilson *B*-value (Å^2)	40	53	71	48
RMSD from ideal geometry				
Bond length (Å)	0.005	0.002	0.004	0.006
Bond angle (°)	0.76	0.57	0.69	1.04
Ramachandran statistics (%)				
Favored	98.7	94.9	97.6	97.6
Outliers	0.0	0.0	0.0	0.0
PDB code	8SIQ	8SIR	8SIS	8SIT

Table S3. X-ray data collection and refinement statistics-continued

Data collection	CC25.4 + SARS-CoV-2 RBD	CC25.43 + SARS-CoV-2 RBD	CC25.56 + SARS-CoV-2 RBD
Beamline	APS23ID-B	APS23ID-B	APS23ID-D
Wavelength (Å)	1.0332	1.0332	1.0332
Space group	P 1 2_1 1	C 1 2 1	C 1 2 1
Unit cell parameters			
a, b, c (Å)	58.2, 143.0, 82.9	311.9, 83.8, 74.1	171.1, 105.6, 99.0
α, β, γ (°)	90, 94.1, 90	90, 100.8, 90	90, 117.3, 90
Resolution (Å) [a]	82.7-1.79 (1.82-1.79)	153.2-2.71 (2.76-2.71)	77.8-2.84 (2.89-2.84)
Unique reflections [a]	126,496 (6,298)	47,774 (2,451)	36,671 (1,820)
Redundancy [a]	7.0 (6.5)	5.2 (5.2)	4.3 (4.2)
Completeness (%) [a]	99.2 (98.6)	93.4 (96.8)	99.1 (98.8)
$\langle I/\sigma_I \rangle$ [a]	9.8 (0.7)	7.8 (1.0)	6.2 (1.1)
R_{sym} [b] (%) [a]	9.4 (>100)	16.5 (>100)	24.7 (>100)
R_{pim} [b] (%) [a]	3.8 (>100)	7.8 (98.4)	13.6 (96.7)
$CC_{1/2}$ [c] (%) [a]	99.8 (35.6)	99.5 (49.5)	97.1 (36.4)
Refinement statistics			
Resolution (Å)	54.1-1.79	72.8-2.71	47.7-2.84
Reflections (work)	125,886	47,703	36,574
Reflections (test)	12,469	4,945	36,05
R_{cryst} [d] / R_{free} [e] (%)	18.6/21.8	26.0/30.4	24.6/28.3
No. Fab/RBD copies in ASU	2	2	2
No. of atoms	10,521	9,536	9,606
RBD	3,149	3.006	3,118
Fab	6,528	6,530	6,447
Ligands [f]	64	0	0
Solvent	780	0	41
Average *B*-values (Å^2)	43	89	55
RBD	42	128	71
Fab	44	71	73
Ligands [f]	60	N/A	N/A
Solvent	46	N/A	51
Wilson *B*-value (Å^2)	32	61	55
RMSD from ideal geometry			
Bond length (Å)	0.010	0.004	0.004
Bond angle (°)	1.1	0.77	0.87
Ramachandran statistics (%) [g]			
Favored	96.3	96.7	97.3
Outliers	0.32	0.16	0.24
PDB code	8SDF	8SDG	8SDH

[a] Numbers in parentheses refer to the highest resolution shell.

[b] $R_{sym} = \Sigma_{hkl} \Sigma_i | I_{hkl,i} - \langle I_{hkl} \rangle | / \Sigma_{hkl} \Sigma_i I_{hkl,i}$ and $R_{pim} = \Sigma_{hkl} (1/(n-1))^{1/2} \Sigma_i | I_{hkl,i} - \langle I_{hkl} \rangle | / \Sigma_{hkl} \Sigma_i I_{hkl,i}$, where $I_{hkl,i}$ is the scaled intensity of the ith measurement of reflection h, k, l, $\langle I_{hkl} \rangle$ is the average intensity for that reflection, and *n* is the redundancy.

[c] $CC_{1/2}$ = Pearson correlation coefficient between two random half datasets.

[d] $R_{cryst} = \Sigma_{hkl} | F_o - F_c | / \Sigma_{hkl} | F_o |$ x 100, where F_o and F_c are the observed and calculated structure factors, respectively.

[e] R_{free} was calculated as for R_{cryst}, but on a test set comprising 2.5% or 5% of the data excluded from refinement.

[f] Bound ligands are MPD.

[g] From MolProbity [84].